Investigating the Impacts of Mixed Layer Depth on Climate Sensitivity

Galen Hall

July 10, 2020

Abstract

The oceanic mixed layer plays an important role in the global climate system as a gateway between the atmosphere and the deep ocean. Yet modelling the mixed layer is difficult, and climate models in the Coupled Model Intercomparison Project ensemble have historically not captured the mixed layer's depth either accurately or precisely, and a wide inter-model variation in mixed layer depths exists (Huang et al., 2014). In light of these wide variations, and in view of the large range of climate sensitivities found in the CMIP6 ensemble, I ask: could variations in mixed layer depth explain some of the variation in climate sensitivity? I test one hypothesis, that the mixed layer relates directly and linearly to the global transient climate response, and find it unsupported. Using a two-box model to estimate climate sensitivity and ocean heat uptake efficacy, I then find that for the subset of CMIP6 models studied here, a strong *negative* correlation between mixed layer depth and short-term climate response exists, as well as a weaker positive correlation between mixed layer depth and equilibrium climate sensitivity, and ocean heat uptake efficacy. A potential explanation for this result is proposed, though further research will be needed to assess it.

Chapter 1

Introduction

The study of the global climate system has become one of the more critical scientific endeavors of the twenty-first century. As greenhouse gases emitted primarily from human activities increase their concentration in the atmosphere, the resulting radiative imbalance causes the atmospheric temperature to rise. This much can be predicted from a simple model: to leading order, the climate approximates a simple energy-balance system, in which short-wave radiation is absorbed from the Sun and emitted as long-wave radiation, through the Stephan-Boltzmann law. The resulting climate change is traditionally measured by the change in global mean surface temperature (hereafter ΔT_s).

Both the important consequences of this temperature change and the mechanisms that determine its exact magnitude are complicated and involve large uncertainties. Understanding and predicting those interactions becomes increasingly important as the magnitude of climate change grows. This task also requires a tremendous amount of information, because the radiative imbalance that causes climate change is coupled to other changes throughout the climate system — and human society — in complex interactions.

A central task of climate scientists therefore involves aggregating large

global datasets of climatic observations and attempting to relate them to past or predicted changes to the radiative imbalance. Physical theory can help to point scientists towards likely interactions and impose fundamental constraints on climate models. For example, conservation of energy along with basic radiative transfer theory can suffice to give a relatively accurate (empirically parameterized) one-dimensional model of the global temperature's response to radiative imbalance. Even with these constraints, however, climate scientists are generally left attempting to interpret the chaotic motions of highly non-linear systems with an enormous number of couplings between variables. It therefore becomes crucial to see which of those interactions can be approximated by a simpler relationship than the fully coupled one, both for the sake of computational efficiency and to build a comprehensible physical picture of the climate system.

One such interaction involves the depth of the mixed layer of the ocean. The ocean can be modelled very roughly as being stratified into the upper mixed layer and the oceanic depths. The mixed layer is a region of seasonally and geographically variable depth beginning at the sea surface and characterized by vertically quasi-uniform density and temperature due to surface-forced mixing turbulence by convection, winds, and waves (Thorpe, 2007). The ocean temperature drops off exponentially below the mixed layer. Both sections of the ocean are important for modulating the global atmospheric surface temperature on different timescales. Roughly, the mixed layer's heat absorption affects temperature changes on decadal–to–century timescales, and the heat absorption of the oceanic depths sets the temperature changes due to radiative imbalance over millennial timescales.

The sea surface mixed layer is small relative to the rest of the ocean: a typical mixed layer depth is 150 m, while the average ocean sea floor depth

globally is about 3700 m. Despite its size the mixed layer plays at least two important roles in regulating the global climate system. First, it acts as a "gateway" between the atmosphere and the deep ocean. Exchanges of heat, momentum and energy between the two atmosphere and the oceanic abyss ultimately set the timescale of global warming; variations in their magnitude and distribution between climate models can help explain differences in climate sensitivities. Second, the mixed layer directly interacts with the atmosphere on short timescales (years to decades), meaning that it directly regulates atmospheric temperatures as well, rather than only through connection to the deep ocean.

In this thesis, I investigate whether a linear approximation of the theory relating mixed layer temperature sensitivity to forcing and mixed layer depth can be extended to predict differences in the global surface temperature sensitivities of climate models. The full theory relating mixed layer depth to climate sensitivity involves difficult nonlinear terms and is not of much use for climate scientists wishing to simplify their predictive and computational work. However, simpler versions of that theory are straightforward and linear. In its simplest form, the depth of the mixed layer relates to the temperature sensitivity defined with respect to the local mixed layer temperature through the following equation:

$$\frac{dT_{os}}{dt} = \frac{F_o}{c_s h} - \lambda_o T_{os}, \tag{1.0.1}$$

where T_{os} is the mixed layer temperature perturbation, λ_o is the mixed layer temperature sensitivity to forcing, F_o is the forcing due to heat flux at the air-sea interface, c_s is the heat capacity per unit depth of the mixed layer, and h is the depth of the mixed layer (Frankignoul and Hasselmann, 1977). The forcing here is defined as a perturbation above the forcing f_1 at which heat flow is balanced. Because the mixed layer is a much larger heat reservoir than the

atmosphere, a relation governing its temperature may hold reasonably well for the atmospheric temperature — at least, an assumption of this sort motivates the investigation. The sea surface temperature (SST) is often the same as the mixed layer temperature to within some small deviation, by definition of the mixed layer, and there is a direct observed proportionality between SST and the global surface air temperature on decadal timescales. Therefore, if this relation holds on decadal timescales for the mixed layer temperature, then it may also be able to relate the sensitivity of the entire climate system to the mixed layer depth.

We should note from the start that using (1.0.1) in this way entails making a number of conceptual leaps. Although the equation closely resembles the energy budget equations used in section 2.1 to develop a basic conceptual model of global warming, there are some notable differences. First, the heat flux F_o above is not the same as the global average radiation flux at the top of the atmosphere (TOA), which is used as the measure of total forcing on the climate system; instead it applies locally at the sea surface. Additionally, equation 1.0.1 is derived assuming constant mixed-layer depth, when in fact the mixed layer depth varies considerably over space and time. The relation above therefore technically holds not as a global relation but only locally, and at specific times. Throughout much of this thesis I nevertheless use globally-averaged statistics which eliminate the geographic variation in all parameters. Held et al. (2010) show that there is time variation in the globally averaged feedback parameter λ_s which Armour et al. (2013) demonstrate can be explained well by geographically localized climate sensitivities ($\lambda(r)$) which are constant in time along with a changing pattern of surface warming. In other words, neither time nor spatial homogeneity in these variables hold in truth, but I will for the most part assume that they do.

We want to see whether this series of conceptual leaps can relate the global average mixed layer to the global average temperature change. Why would this be an important finding? First, any explanation of variation in climate sensitivities between models is helpful, as it allows modellers to focus on those variables which it is most important to parametrize accurately (relative to their real-world values). Second, the potential effects of variations in mixed layer depth have generally faded from primary relevance among researchers, but perhaps more because of quirks in the history of model development than any conclusive evidence that such effects don't exist. Finally, the most recent set of models in the Coupled Model Intercomparison Project — the CMIP6 ensemble — feature some models with surprisingly high climate sensitivity. Other researchers have explained part of these high sensitivities as due to greater aerosol sensitivity, which in combination with historical and present-day aerosol observations effectively places an *emergent constraint* on the climate response (Nijsse et al., 2020). An emergent constraint is a robust linkage between higher-order processes or parameters in the climate system which allows researchers to constrain the range of realistic sensitivities by taking as accurate only those models that conform well to the real values of these parameters, historically. But there are inter-model differences not explained by this effect. If different mixed layer depths contribute in the way hypothesized, then we could assess the feasibility of those concerningly high sensitivities based on how well their mixed layers conform to expected values, in effect finding another emergent constraint on climate sensitivity.

The basic task of this thesis is therefore to look for a significant correlation between mixed layer depth and climate sensitivity, and, if such a correlation exists, to assess whether it conforms roughly to the linear approximation in equation 1.0.1, or whether there must be some other explanation. Our null hy-

pothesis is that local ocean surface temperature variability depends on mixed layer depth, but that variations due to anthropogenic forcing dwarf this effect, so that there is no detectable relationship between the mixed layer depth and climate sensitivity.

The thesis proceeds in three chapters. In chapter 2: **A Simple Model of Climate Change** I build a simple picture of the climate system, starting with the most basic energy balance models and then including processes of ocean heat content and heat transfer within the system, as well as an explanation of the radiative transfer process which warms the atmosphere after an increase in top-of-atmosphere downwards radiative forcing.

In chapter 3: **Mixed Layer Theory** I review background on modelling the variability of mixed layer depth and its effect on temperature and ocean heat transfer. I introduce the theory in Frankignoul and Hasselmann (1977). And I review a small section of the literature on different modelling parameterizations which affect mixed layer depth.

In the third and last chapter, 4: **Mixed layer depth and climate sensitivity**, I cover the main findings: after fitting a two-box model to calculate climate sensitivity and heat uptake efficacy (Geoffroy et al., 2013*a*; Gregory, 2000), I find that mixed layer depth does not correlate strongly with near-term transient climate response, but shares surprisingly strong correlations with the equilibrium response and the ocean heat uptake efficacy. I review some possible explanations for these counterintuitive correlations. Ultimately they remain an open question and an avenue for further research.

CMIP6 climate models & methodology

The Intergovernmental Panel on Climate Change (IPCC) is the global hub for climate research. The IPCC is tasked with, among other things, predicting

the likely range of temperature changes resultant from various hypothetical emissions "scenarios," as well as the various changes in the climate system that we can expect to accompany a given temperature change. It is generally assumed that most important changes to things like precipitation, vegetation, glaciation and so forth track temperature changes, so having a reasonable estimate of the future temperature change is critical. While simple models of climate change such as those in Sections 2.1-2.2 can approximate most of the important characteristics of temperature change in response to linearly increasing forcing (which roughly describes the forcing resultant from historical human emissions) much more complex models are required to predict changes to local conditions. The IPCC relies on the Coupled Model Intercomparison Project (CMIP) (Taylor et al., 2012; Eyring et al., 2016), which assembles a host of atmosphere-ocean general circulation models (AOGCMs) and Earth System Models (ESMs).

Parameterizations of sub-grid-scale dynamics in AOGCMs can impact the large-scale model behavior. AOGCMs incorporate dozens or hundreds of variables and represent the climate system in 3+1 dimensions, building in (ideally) all relevant processes at all calculable scales. In practice a typical horizontal resolution for ocean process calculations is 100km $\times$ 100km or 1°$\times$ 1°. Computation excludes the possibility of emergent dynamics at scales near or below grid-scale; instead phenomena on length scales smaller than 100km must be parameterized directly in the model. The various ocean and atmospheric turbulence processes that contribute to mixed layer depth comprise one set of directly parametrized processes, although there are many others. These parameters can also be fine-tuned by comparing the output of a model run on a simulation of historical emissions against the real historical temperature record. Since 2005 the Argo observing network of profiling ocean floats has

been active globally, allowing comprehensive comparison of modeled ocean dynamics and stratification with the real world (Argo, 2020). Flato et al. (2013) look in-depth at the variations between climate models in the CMIP5 ensemble. Among other things, they find that there is a step-change in accuracy of some modelled ocean dynamics for models that can resolve the sub-mesoscale, which reinforces the above point.

The Fifth Assessment Report of the IPCC was released in 2013 and 2014 using the CMIP5 ensemble of AOGCMs. Working Group 1 reported a likely range for the ECS calculated from the ensemble of CMIP5 models of 1.5 - 4.5°C (Collins et al., 2013). This estimate has not changed significantly over several decades of modelling, although the ability of models to predict the concomitant impacts from a given amount of warming has improved. Prior to the release of AR5, Hansen et al. (2011) remarked that most AOGCMs were mixing heat into the deep ocean too efficiently and therefore underestimating the amount of negative forcing generated by human-made aerosols. Climate models must be calibrated against historical data, so there is no way to directly calculate the ECS within the calibration. As a result, only the transient climate sensitivity can be used to calibrate. Whereas the ECS assumes that the temperature response of the oceans has reached equilibrium, the transient response depends on the *rate* of temperature change of the oceans, so changes in this rate can counteract changes in the radiative forcing in the model and therefore hide discrepancies with the historical data. In other words, "the potentially compensating influences of the uncertain climate sensitivity and the magnitudes of the cooling forcings" make it difficult to accurately estimate the climate sensitivity from historical forcing (Winton et al., 2020).

Conversely, some of the CMIP6 and CMIP5 climate models have been criticized for *overestimating* the transient and equilibrium climate sensitivi-

ties. Winton et al. (2020) show that in the case of GFDL's CM4.0 model, the climate sensitivities are on the higher end despite conforming to historical temperature and forcing data because the model's high sensitivity to greenhouse gases was masked by its high sensitivity to aerosols over the historical runs. The Community Earth System Model Version 2 (CESM2) also has a high equilibrium climate sensitivity of 5.3 K, which is an increase of 0.9 K on previous iterations of the model. In this case the increase has been attributed to a higher cloud feedback sensitivity by Gettelman et al. (2019).

In each case, a simple energy balance approach along the lines of equation (2.1.17) underestimates the climate sensitivity because variations in one part of the more complicated model cancel out variations in another part within the historical simulation. However it is also possible that effects such as this could arise in places other than the cloud feedbacks or aerosol sensitivities. This speculation forms part of the motivation for investigating differences in mixed layer depth in the current study.

1.1 Data sources and methods

All of the data for this thesis comes from the Earth System Grid Federation's (ESGF) database of CMIP6 model outputs, and some was accessed using `pangeo`'s Google Cloud mirror of ESGF's database. The variables used include surface temperature, T_s (`ts` in the CMIP6 vocabulary); sea surface temperature, T_{os} (`tos`); net TOA radiation flux, F_a (`rtmt`); net ocean surface heat flux, F_o (`hfds`); and mixed layer depth, h (`mlotst`). They were retrieved as `netcdf` files and in most cases global averages were taken over the entire time period prior to analysis. Global averages were calculated as the weighted average of the given value over all grid points, for each time step, with the weights being the latitude at the center of each grid point. All data sets had

one-month time steps. Data processing was carried out in python.

The forcing scenarios used in this thesis are:

1. `1pctCO2`: atmospheric CO_2 concentration steadily increase at 1% per year up to $4 \times \rho(0)$, so that the net TOA forcing approximately quadruples by year 140.

2. `abrupt-4xCO2`: atmospheric CO_2 is quadrupled at year 0.

3. `piControl`: the control run set to mimic the preindustrial climate (prior to 1850 AD).

This thesis only uses those climate models for which all of the variables mentioned above were available, for each of the three scenarios. In cases where there were redundant climate models (e.g. a high resolution and a low resolution version) only one of the set was included. Additionally due to time and technical constraints, several viable models were not included — this was primarily because they were too slow to download over standard internet connections.

The final list comprises the following models, given by their `source_id` in the ESGF database. Each has a unique color and symbol combination that are used throughout the rest of the thesis.

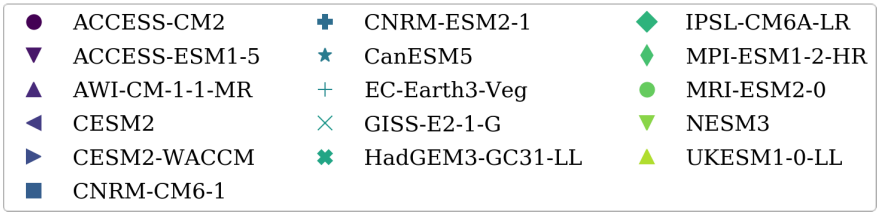

Figure 1.1: The GCMs used in this thesis with their corresponding markers.

Chapter 2

A Simple Model of Climate Change

Although the global climate system is very complicated, some of its core characteristics can be explained using relatively simple models. Here I use a basic energy-budget model to explain the mechanisms causing global warming, and I include a quick explanation of radiative transfer, feedbacks, and global warming timescales.

I then explain how climate models work and the role they play in this investigation. Climate modelling began in a simplified sense well in advance of modern weather forecasting — through simple energy budget models — but modern global coupled climate models are far more complex and can use cells on the order of 100km lengths. Importantly, the resolution of modern climate models still leaves turbulence below this resolution to be parametrized by researchers.

The ocean plays a central role in setting the rate of global warming because of its enormous heat capacity relative to the atmosphere. At different timescales, different depths of the ocean have greater or lesser impact on the

atmospheric temperature because of the differing times it takes for changes in radiative forcing to affect the deep (shallow) ocean temperature, and the times necessary for those changes to percolate back to the atmosphere. The oceanic mixed layer interacts with the atmosphere far faster than the depths do, which means that the mixed layer temperature should impact the rate of warming in the lower atmosphere on short timescales. I review a basic theory of this interaction and also explain some of the key sources of turbulent mixing in the surface of the ocean, and how they can vary among climate models.

Symbol	**Name**	**Scenarios**	**Calculation**
ECS or $\Delta T_{2\times}$	equilibrium climate sensitivity	`abrupt`	$\Delta T_s(N=0)/2$ (Gregory, 2004)
λ_{eq}	equilibrium climate feedback parameter	`abrupt`	$-\frac{dN}{dT_s}$ (Gregory, 2004)
ERF or $F_{2\times}$	effective radiative forcing	`abrupt`	$N(\Delta T_s=0)/2$ (Gregory, 2004)
TCR	trasient climate sensitivity	`1pct`	$\overline{\Delta T}(61-80yrs)$
$\Delta T_{2\times,\text{eff}}$	effective climate sensitivity	`1pct, abrupt`	$\frac{F_{2\times}\Delta T_s}{F(t)-N(t)}$
κ	ocean heat uptake efficiency	`1pct`	$\frac{N}{\Delta T_s}$
ϵ	ocean heat uptake efficacy	`1pct, abrupt`	$\frac{(\Delta T_{eq}-\Delta T_s)/N}{\Delta T_{eq}/F}$
$C_{\text{eff},s}$	effective heat capacity	`1pct, abrupt`	$\int_{t'=0}^{t} N(t')dt'/\Delta T_s$

Table 2.1: The variables calculated in this thesis. **Scenario** indicates the CMIP6 scenarios whose output was used to calculate the corresponding variable. Note that all variables could be calculated twice: first using the global surface temperature `ts` as a reference and second using the ocean surface temperature `tos`. (The subscripts above correspond to the surface temperature.) In all cases except ECS and TCR, the variables were calculated for each time-step using 10-year rolling averages of the relevant variables entering the calculation to remove noise. κ was calculated as the slope of the $N-\Delta T$ relationship, with $\kappa(t)=\overline{dN(t')/d\Delta T(t')}$ for $t'\in[0,t]$. ϵ was calculated first using the equation shown, and then using the methods from Geoffroy et al. (2013*b*,*a*).

2.1 Basic theory: radiative transfer, feedbacks, and global warming timescales, energy balance models

The Earth's climate is fundamentally governed by the relationship between the energy entering the Earth system from outer space, and the energy leaving it. If we include the entire Earth in our definition of the "climate system," then energy can ultimately only leave as radiation. (If we were to look at only the atmosphere, for example, then the deep ocean would be a significant energy sink.) The primary source of incoming energy is sunlight. The Earth's energy balance arises when the power emitted by black-body radiation from the Earth equals the power absorbed from that sunlight. This is a basic constraint on the climate system and any attempts to model it; black body radiation ultimately provides a restoring feedback on any energy imbalance so that the system tends back towards equilibrium. The entire goal of climate modelling lies in predicting what changes the Earth's climate will undergo in the process of recovering that equilibrium, and how fast it will do so. To say more about this we need a brief review of the physics of global warming. Although this thesis focuses on ocean dynamics some background on radiative transfer and the structure of the climate system is generally useful. The derivations in this section are based on those in Marshall and Plumb (2008) and Allen (2019) with some modifications.

Earth-Sun energy balance

One can approximate the surface temperature of the Earth very roughly using a simple black-body argument. The Sun emits as a black-body with temperature 5770K. The flux of energy per meter squared, F, from a black-body is

given by the Stefan-Boltzmann Law:

$$F_{sun} = \sigma T^4, \quad \sigma = \frac{2\pi^5 k^4}{15c^2h^3} \tag{2.1.1}$$

where k is the Boltzmann Constant, h is Planck's Constant, and c is the speed of light. Numerically, the Stefan-Boltzmann constant $\sigma = 5.67 \times 10^{-8} Wm^{-2}K^{-4}$. The Sun is a distance $S_0 = 150 \times 10^9$m from the Earth (averaged throughout the Earth's elliptical orbit), and radiation from the Sun "sees" a circular Earth of radius $R_e = 6.371 \times 10^6$m and surface area 1/4 the total surface area of the Earth. Dividing F by the area of the spheroid with radius S_0 and multiplying by 1/4 we obtain the power per unit area incident on the Earth from the Sun, 342 W m^{-2}.

Of the incident radiation about 30% is reflected due to Earth's albedo, α. Treating Earth as a black-body with temperature T_e, at radiative equilibrium the Stefan-Boltzmann Law gives us:

$$F_{Earth} = \sigma T_e^4 \tag{2.1.2}$$

$$= 342 \text{ Wm}^{-2} \times (1 - \alpha) \tag{2.1.3}$$

Solving for T_e with $\alpha = 0.30$ gives a temperature of 255K, approximately 33K below the true global average surface temperature. This 33K difference, equivalent to a "natural" forcing of 150 Wm^{-2}, is due to the presence of the greenhouse gases in the atmosphere. While the temperature that the Earth displays to outer space truly is approximately 255K, greenhouse gases make the lower atmosphere opaque to radiation and elevate the level from which radiation can escape to space to higher, colder altitudes. The surface of the Earth becomes warmer through this process, which is called radiative transfer. Note that throughout the process of reaching equilibrium following an increase in net downwards forcing, the albedo of the earth might change

both at the surface and in the atmosphere. Feedbacks such as this will be discussed shortly.

Radiative Transfer

Greenhouse gases are those constituents of the atmosphere which can absorb and emit photons at wavelengths relevant to the Earth's total irradiance. These are the tri-atomic gases, such as H_2O and CO_2, which are the two most important in terms of their contribution to atmospheric absorption. These gases have vibratory modes at which their structure forms a dipole which is capable of emitting and absorbing photons. We will focus on CO_2 because its concentration is set by emissions from human activity along with some natural feedbacks and yearly cycles, which we ignore here. The following derivations roughly track those in Andrews (2010).

At the pressures and temperatures observed in the atmosphere, dry air follows near-ideal gas behavior. At global scales we can treat the vertical acceleration in the atmosphere as secondary because the atmosphere is much wider than it is tall. In this case the hydrostatic approximation holds, which says that:

$$\frac{dp}{dz} = -g\rho \tag{2.1.4}$$

Here p is the pressure, z is the height (increasing vertically), g is the acceleration due to gravity and ρ is the density of the gas. We can see that this holds because for an infinitesimal slab of gas with no net acceleration and therefore no net force applied, $g\rho\delta z = p(z) - p(z+\delta z)$. As δz approaches zero this becomes equation (2.1.4). For an ideal gas $pV = nRT$, where V is the volume, n the number of moles of gas, R the universal gas constant and T the temperature.

We can rewrite the ideal gas law in terms of the molar mass of dry air to obtain:

$$p = \rho R_a T \tag{2.1.5}$$

Here $R_a = R/m_a$ and m_a is the molar mass of dry air.

Finally, if we assume that the temperature T is constant, we may rewrite the hydrostatic balance equation (2.1.4) to obtain:

$$\begin{aligned} \frac{dp}{dz} &= -g\frac{p}{R_a T} \\ \frac{d(\ln p)}{dz} &= -\frac{g}{R_a T} \\ p &= p_0 \exp\left(-\frac{gz}{R_a T}\right) \end{aligned}$$

Although the temperature of the atmosphere is not exactly constant, this exponential decrease in pressure is approximately correct within the troposphere. Defining the pressure scale height $H = R_a T/g$, we can write:

$$p = p_0 e^{-z/H}. \tag{2.1.6}$$

H is roughly 8 km throughout most of the troposphere.

Now we have about enough information to define a basic model of radiative transfer. The optical thickness of a given slab of atmosphere with thickness δz for a given wavenumber of light ν is given by

$$\delta\tau_\nu \propto k_\nu \rho \delta z \tag{2.1.7}$$

The constant of proportionality is of order one and we can ignore it for our purposes. The change in upwards irradiance through a slab of atmosphere is given by Lambert's and Kirchoff's laws:

$$\delta I_\nu = I_\nu \delta\tau_\nu - \pi B_\nu(T)\delta\tau_\nu \tag{2.1.8}$$

Where πB_ν corresponds to the Planck function for the temperature of the given slab integrated over a hemisphere to account for upwards emission in all directions; we can call this the *brightness temperature*. The first term corresponds to absorption and the second to emission, and the minus sign is present because $\delta\tau_\nu$ is negative in the upwards direction. The transmittance $\mathcal{T}_\nu(z)$ of a given wavelength of light is equal to the percent of light at that wavenumber emitted from an altitude z that would reach infinity without being absorbed. In the absence of the second (emitting) term above, we can define it as $I_\nu(\infty)/I_\nu(z)$ and write:

$$d\tau_\nu = dI_\nu/I_\nu \tag{2.1.9}$$

$$\tau_\nu(z) = \int_{\tau'_\nu(z=\infty)=0}^{\tau'_\nu(z)} d\tau'_\nu \tag{2.1.10}$$

$$= -\ln \mathcal{T}_\nu(z) \tag{2.1.11}$$

To a good-enough approximation, the optical depth τ_ν decreases exponentially with height and the Planck function $B(\nu)$ decreases approximately linearly with height in the troposphere, and is constant in the quasi-isothermal stratosphere, assuming a near-constant temperature lapse rate in the atmosphere and near-constant dB/dT. From equation (2.1.7), the optical depth is proportional to ρ. This leaves us with the key conclusion: for a doubling of the density of a given well-mixed greenhouse gas, say CO_2, the optical depth is displaced upwards by an amount proportional to $\ln(2)$ and the Planck function is reduced by an amount proportional to $\ln(2)$. In other words, doubling the amount of CO_2 in the atmosphere causes a logarithmic increase in the average height of transmittance, and therefore a logarithmic decrease in the average

irradiance. To make up for that decrease, the atmosphere has to warm up until the CO_2 at this higher level is warm enough for the emittance to again balance the incoming radiation from the Sun. Each sequential doubling of CO_2 should produce roughly the same total temperature change.

Although there are many important caveats to this picture, it suffices to explain the cause and scale of the warming that we observe in climate models upon an instantaneous doubling or quadrupling of CO_2 concentrations. Carrying the derivation further and averaging over all wavelengths, one would find that the reduction in top-of-atmosphere (TOA) outgoing irradiance due to a doubling of CO_2 concentration generates a reduction in net upward radiant energy flux $F_{2\times} = 3.7\text{Wm}^{-2}$. This forcing tells us relatively little about the resultant temperature change at either short or long timescales, however, because that change depends on the complex response of the global climate system to this increase in forcing.

Feedbacks and the equilibrium response

Many negative impacts from climate change scale approximately with the surface temperature of the atmosphere. Guided by goals set in international agreements, a central job of climate scientists is to (1) predict the amount of surface warming that will result from a given amount of carbon emissions and (2) associating those temperature increases with other predicted changes in the global climate. Difficulties arise immediately, because the rate of temperature change in response to forcing — or equivalently, the amount of forcing restored per unit increase in temperature — is fiendishly difficult to predict.

If we were to again treat the Earth as a simple black-body with a temperature T_e defined as the average brightness temperature of the Earth, then negating a decrease in net upwards radiative forcing of 3.7Wm^{-2} would re-

quire warming the atmosphere uniformly by about 1K. In practice this does not happen; surface temperatures are only tied very indirectly to the brightness temperature that sets the irradiance. We can parameterize the increase in net upwards irradiance that occurs from an increase in surface temperature using:

$$\lambda_s \equiv \frac{dF_{earth}}{dT_s} \tag{2.1.12}$$

If we knew λ, then calculating the final surface temperature change from an initial sudden increase in CO_2 concentration would be straightforward. In order for the change in temperature ΔT_s to balance the Earth's energy budget, we would need:

$$(F_{2\times})\frac{\ln \rho_f}{\ln \rho_i} = \int_{T_i}^{T_f = T_i + \Delta T_s} \lambda_s dT_s \tag{2.1.13}$$

Where ρ_f is the final concentration of CO_2, ρ_i the initial concentration, and the integral accounts for possible variation of λ_s with temperature. Realistically λ_s does change both with time and geographically (Held et al., 2010; Armour et al., 2013). The logarithms enter because of the logarithmic dependence of the irradiance on temperature outlined in the previous section. If we treat λ_s as a constant, we can turn this implicit equation for ΔT_s into an explicit one:

$$\lambda_s \Delta T_s = F \tag{2.1.14}$$

Here we have simply substituted F for the forcing imbalance. We then define the *equilibrium climate sensitivity* (ECS) as the final change in temperature at radiative equilibrium resulting from a sudden doubling in atmospheric CO_2:

$$\Delta T_{2\times} \equiv \frac{F_{2\times}}{\lambda_s} \tag{2.1.15}$$

Predicting the ECS requires knowing λ_s. But λ_s depends on a number of factors, some of which are not well-understood. One such factor is cloud cover: since clouds contribute significantly to the Earth's albedo, and some

clouds also trap heat in the atmosphere, understanding how cloud formation will change due to an increase in radiative forcing is important for estimating λ.

The feedbacks that contribute to set λ_s are for the most part nonlinear and intercoupled. Summing up all the different sources of uncertainty can give us a fair estimate of the uncertainty in λ_s, but the real spread of ECS predictions is traditionally found using a range of fully-coupled climate models each using different paramterizations. The 2013 IPCC Assessment Report of Working Group 1 found a range of likely predictions for the ECS from 1.5K to 4.5K (Collins et al., 2013). This prediction came out of the Coupled Model Intercomparison Project version 5 (CMIP5) (Taylor et al., 2012). Some newer CMIP6 (Eyring et al., 2016) models for use in the next Assessment Report have reported climate sensitivities far outside of this range (Winton et al., 2020; Gettelman et al., 2019; Nijsse et al., 2020). This discrepancy has motivated a search for explanations as to why these large model biases (if they are biases) arose, which this thesis hopes to contribute to.

A climate model typically takes between hundreds and thousands of years to reach equilibrium after a sudden increase in forcing, due to the slow adjustment of the cryosphere and deep oceans. But it is also often useful to know how the climate (or model) responds to steadily increasing forcing over time. Energy conservation gives the following equation for the global energy budget:

$$N = F - \lambda_s \Delta T_s \tag{2.1.16}$$

where N is the rate of heat uptake by the climate system, primarily determined by the rate of ocean heat uptake because the heat capacity of the ocean $C_o \gg C_a$; F is the forcing prior to readjustment by the climate system, and all values are perturbations on equilibrium at which we assume there is no net heat flux into the climate system. By combining equations (2.1.16) and

(2.1.15), we obtain an approximate equation for $\Delta T_{2\times}$:

$$\Delta T_{2\times,\text{eff}} = \frac{F_{2\times}\Delta T}{F - N}. \tag{2.1.17}$$

We call $\Delta T_{2\times,\text{eff}}$, which was introduced by Murphy (1995), the *effective climate sensitivity*. This is far from an exact equation, however, because we have been treating λ as a constant even though internal climate variability causes it to change as the climate system equilibrates. In other words, equation (2.1.17) only incorporates information about λ prior to the period in which temperatures begin to converge (otherwise $Q \approx 0$). It turns out that as temperatures do converge, λ becomes smaller and these effects are too significant to ignore (Allen, 2019; Winton et al., 2020). However, with more information about the climate system we can use equation (2.1.16) to construct a simple and fairly accurate model of the Earth's response to increasing forcing.

2.2 Ocean heat content and the rate of warming

The rate of heat entering the climate system, N, can be decomposed into the changes in temperature of the various segments of the climate system multiplied by their respective heat capacities. Since the atmosphere's heat capacity is equivalent to the upper 3 m of the ocean, we can create a simple two-box model of the climate system including only the deep ocean and the shallow ocean as heat reservoirs. The shallow ocean has a temperature which we will also term T_{os}, counting on the fact that the temperature of the ocean surface roughly corresponds to the global surface temperature because the top layers of the ocean are such a large heat reservoir compared to the atmosphere. The deep ocean temperature we term T_d, and we write corresponding heat capacities for both bodies c_s and c_d. This approximation is fairly accurate on large scales, since the oceanic thermocline is usually stably stratified and

the deep ocean is therefore a distinct body from the upper ocean. Various processes contribute to a net heat transport H from the warmer surface ocean to the cooler deep ocean. One large-scale process which contributes to H is the overturning circulation, whereby cold polar water sinks into the oceanic depths, cooling them and creating a pressure front that expands equatorward (see Marshall and Plumb, 2008, Chap. 11; Vallis, 2019, Chap. 15).

We can construct a simple two-box model of this process following Held et al. (2010) and Gregory (2000), ignoring additional diffusion terms:

$$c_s \frac{d(h\Delta T_{os})}{dt} = -\lambda_{os}\Delta T_{os} - H + F, \tag{2.2.1}$$

$$C_d \frac{d\Delta T_d}{dt} = H. \tag{2.2.2}$$

Here, ΔT_{os} is the perturbation to the global mean surface temperature, c_s is the heat capacity per unit depth of the mixed layer of the ocean which responds rapidly to changes in the atmosphere, h is the height of the mixed layer (allowing for time variation), ΔT_d is the perturbation to the temperature of the deep layers of the ocean which possess a cumulative heat capacity C_d, and H is the heat exchange between the two segments of the ocean. We have written λ_{os} to indicate the climate sensitivity parameter in terms of the ocean surface temperature rather than the surface air temperature – however if changes to the two are assumed to be proportional, all of the *os* subscripts in equation (2.2.1) could be replaced with s for atmospheric values.

We assume that H is proportional to the temperature difference:

$$H = \gamma(\Delta T_{os} - \Delta T_d), \tag{2.2.3}$$

And further assume (for now) that h is constant so we can write $C_s = c_s h$ and remove h from the derivative. At equilibrium $H = 0$ so $\Delta T_{os} = \Delta T_d =$

F/λ. We define the fast (surface) relaxation time $\tau_s \equiv C_s/(\lambda_{os} + \gamma)$, and as long as F varies on timescales much larger than τ_s, we ignore the derivative in (2.2.1) so that

$$\Delta T_{os} \approx \frac{F + \gamma T_d}{\gamma + \lambda_{os}} \tag{2.2.4}$$

in which case the evolution of the deep ocean temperature becomes

$$C_d \frac{d\Delta T_d}{dt} \approx -\frac{\lambda_{os}\gamma}{\lambda_{os} + \gamma}\Delta T_d + \frac{\gamma}{\lambda_{os} + \gamma}F \tag{2.2.5}$$

and ΔT_d relaxes to the equilibrium value F/λ on the slow (deep ocean) timescale

$$\tau_d \equiv \frac{C_d(\lambda_{os} + \gamma)}{\lambda_{os}\gamma}. \tag{2.2.6}$$

On timescales much shorter than τ_d, for which the deep ocean has not responded significantly and we can treat $T_d \approx 0$, the surface temperature can be thought of as responding to the instantaneous forcing alone, with a transient sensitivity defined by

$$\Delta T_{os} \approx \Delta T_F \equiv \frac{F}{\lambda_{os} + \gamma}. \tag{2.2.7}$$

This scheme is important for understanding twentieth-century warming, as described in Gregory and Forster (2008) and covered in greater detail in section 1. However at this point it is important to note that the heat capacity of the upper layer of the ocean does not feature at all in equation (2.2.7). The prior assumption that F varies on timescales much larger than the surface temperature relaxation time τ_s, and further that $\tau_d \gg \tau_s$, mean that in equation (2.2.7) we treat the relaxation time as effectively zero, and therefore set $\lambda\Delta T_{os} + \gamma\Delta T_{os} = F$. In other words, we assume that the upper ocean adjusts so fast to changes in the TOA forcing that its heat capacity c_s does not matter.

Is this a fair assumption? If we make the further assumption that the top-of-atmosphere forcing F over water is equal to the net heat flux into the

ocean surface, which covers approximately 70% of the Earth's surface, we can do a back-of-the-envelope check:

$$\frac{F}{C_s} = \frac{d\Delta T_{os}}{dt} \tag{2.2.8}$$

$$= \frac{3.7 \text{ W m}^{-2}}{\text{MLD} \times 0.7 \times C_{\text{water}} \times \rho_{\text{water}}} \tag{2.2.9}$$

$$\approx 1.5 - 2 \deg \text{K per decade.} \tag{2.2.10}$$

Here we assume that the depth of the mixed layer MLD = 150m, with standard values for the heat capacity and density of water, C_{water} and ρ_{water}. The resulting rate of warming assuming zero climate sensitivity and zero heat transfer to the deep ocean is approximately 2 degrees Kelvin per decade. In this calculation we assume that the upper ocean is responding to a forcing equivalent to an instantaneous doubling of CO_2. We can therefore compare this rate of change to the rate of change in the first few years of an `abrupt-4xCO2` model run. The result is shown in Figure 2.1.

Keeping in mind that we must divide the resultant slopes by 2 to match the calculation in (2.2.8)-(2.2.10), we find that the rate of temperature change over the first decade is approximately equal to F/c_s but drops off quickly afterwards as the temperature feedback term becomes large and can't be ignored. On longer timescales the H term becomes important as well.

What can we infer about the hypothesis that the rate of warming should be inversely proportional to the heat capacity of the surface layer of the ocean? Clearly over timescales $\tau \gg \tau_s$, the heat capacity c_s does not matter very much, except perhaps indirectly. However on decadal to multidecadal timescales, variations in c_s hypothetically have a significant effect on variations in the temperature response ΔT_s both between and within models. In Chapter 3 I look in greater detail at why the mixed layer depth varies between climate models and how that variation could feasibly affect climate sensitivi-

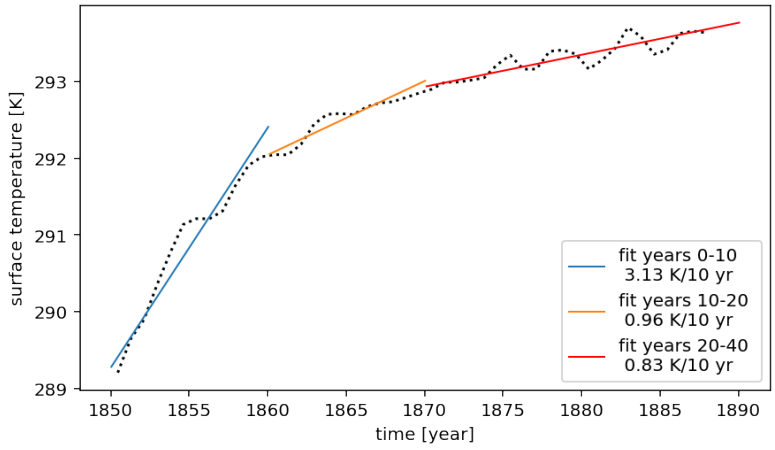

Figure 2.1: The fast response to an abrupt quadrupling of atmospheric CO_2 in the `UKESM1-0-LL` model. In the first decade T_s increases approximately linearly with slope 3.13 degrees Kelvin per decade; in the second decade this slope decreases to 0.96 degrees Kelvin per decade and 0.83 over the third and fourth decades. The black dotted line is a one-year moving average of the temperature.

ties.

Calculating ΔT_{eq} and F

2.3 Time-varying climate sensitivity

The two-box model presented in the previous section has two different timescales on which warming is primarily dependent on either the surface or deep layer of the ocean (τ_s and τ_d respectively). In designing climate models based on historical and present observations, we generally have good data only about the present-day short-term climate response, and we hope to constrain both the future short-term response and the equilibrium response based on that data. Some qualifications to the two-box model can give us the conceptual tools to do so. This section closely follows the summary given in Yoshimori et al. (2016).

Ocean heat uptake efficiency

Under monotonically increasing forcing, as in a `1pctCO2` model run, it is common to approximate the ocean heat uptake as

$$N = \kappa \Delta T_s \tag{2.3.1}$$

where κ is the *ocean heat uptake efficiency* which is assumed to be either constant or slowly varying with ΔT_s (Gregory and Forster, 2008; Winton et al., 2020; Yoshimori et al., 2016). In terms of the model in equations (2.2.1) and (2.2.2), this assumption can be written as:

$$N = C_s \frac{dT_s}{dt} + C_d \frac{dT_d}{dt} = \kappa \Delta T_s \tag{2.3.2}$$

$$= F - \lambda_s \Delta T_s \tag{2.3.3}$$

$$\therefore F = (\lambda_s + \kappa) \Delta T_s \tag{2.3.4}$$

where we have made use of the assumption mentioned in the preceding section that the average ocean surface and surface air temperature are proportional, so we can exchange subscripts *os* and *s* from equation (2.2.1). The resulting equation (2.3.4) allows us to define, following Gregory and Forster (2008), the *climate resistance* $\rho \equiv \kappa + \lambda$. Over periods of transiently increasing forcing, the temperature change should be related to the forcing by $\Delta T_s = F/\rho$.

Equation (2.3.1) can only hold during periods of increasing forcing and on short (i.e. non-equilibrium) timescales. The simplest explanation for this is that as the climate system equilibrates to a constant forcing, $N \to 0$ while ΔT_s approaches $\Delta T_{2\times}$. Conversely, during periods of increasing forcing we expect the ocean heat uptake N to increase proportionally, as the excess forcing has nowhere else to go. $F = \rho \Delta T_s$ has no timescale, so as long as we can treat κ as near-constant this relation should hold (Gregory and Forster, 2008).

The ocean heat uptake efficiency is closely related to the concept of *effective heat capacity*, or the heat capacity of the climate system corresponding to a temperature change ΔT_s after a time t. The effective heat capacity at time t can be defined as

$$C_{\text{eff},s} = \frac{\int_{t'=0}^{t} N(t')\mathrm{d}t'}{\Delta T_s}, \tag{2.3.5}$$

in other words the total time-integrated heat flux into the *entire* climate system to achieve a *surface* temperature change ΔT_s (Donohoe et al., 2014).

Comparison to equation (2.3.1) and (2.3.4) lets us write, over transient forcing timescales,

$$C_{\text{eff},s} = \frac{1}{\Delta T_s}\int \kappa \Delta T_s \mathrm{d}t' \tag{2.3.6}$$

$$= \frac{\kappa}{F(t)}\int F(t')\mathrm{d}t'. \tag{2.3.7}$$

Equation (2.3.7) indicates that a higher ocean heat uptake efficiency corresponds to a faster increase in the effective heat capacity, and therefore either (1) a greater role for the deep ocean over periods of transient warming or (2) a larger surface mixed layer, or both. Conversely, a larger λ_s corresponds primarily to more effective atmospheric feedback processes. $C_{\text{eff},s}$ is an intentionally rough measure, and should not be confused with the *true* heat capacity of the climate system. Rather, it gives an idea of the strength of coupling between ocean heat content and surface temperature change. If $C_{\text{eff},s}$ is large, then the deep ocean is playing a significant role in setting the rate of change of warming.

Finally, we can also use equation (2.3.4) to obtain a relation between the warming during transient forcing and the equilibrium warming, assuming that λ_s is equal to the equilibrium climate sensitivity:

$$\frac{\text{TCR}}{\text{ECS}} = \frac{1}{1+\kappa/\lambda_s}. \tag{2.3.8}$$

Accordingly, if κ is larger, then transient warming should be smaller compared to equilibrium warming.

Using equation (2.3.1) should therefore allow us to compare the relative importance of ocean heat uptake, climate feedbacks, and initial radiative forcing in determining both transient and equilibrium climate sensitivity. However it is important to note that this conclusion relies on assuming that λ_s is constant over time. If there are time-dependent feedbacks, or feedbacks that depend on the absolute magnitude of temperature change, then λ_s may vary significantly with time and the ratio of transient to equilibrium warming may be significantly different than that described by equation (2.3.8).

Ocean heat uptake efficacy

We can compare the transient and equilibrium climate feedback parameters by using the *effective climate sensitivity*, $\Delta T_{2\times,\text{eff}}$, introduced in equation (2.1.17) as an inexact measure of the equilibrium response. Gregory (2004) report that $\Delta T_{2\times,\text{eff}}$ is significantly different from the actual ECS, and a number of studies have since affirmed this claim (Yoshimori et al., 2016). This result indicates that the assumption operative in equation (2.3.8) is wrong: namely, we cannot assume that the ratio between κ and λ_s is constant.

To distinguish the factors affecting the climate response on different timescales, we define the *ocean heat uptake efficacy* following Winton et al. (2010, 2020) and Yoshimori et al. (2016) as

$$\epsilon = \frac{(\Delta T_{eq} - \Delta T_s)/N}{\Delta T_{eq}/F}. \tag{2.3.9}$$

If we then define a sensitivity parameter for the ocean heat uptake, λ_o, as follows:

$$\lambda_o = \frac{N}{\text{ECS} - \Delta T_s}, \tag{2.3.10}$$

we can explain the ocean heat uptake efficacy as the ratio between the equilibrium feedback parameter and the ocean heat uptake feedback parameter,

$$\epsilon = \frac{\lambda_{eq}}{\lambda_o}. \tag{2.3.11}$$

The ocean heat uptake sensitivity λ_o represents the change in surface temperature following an increase in forcing that is due to heat exchange with the ocean, while λ_{eq} incorporates all feedbacks into the equilibrium climate sensitivity parameter. In other words, a smaller ocean heat uptake efficacy indicates that the ocean heat uptake contributes less to the climate response and therefore the transient climate response should be closer to the equilibrium response. A larger efficacy implies the opposite. We can see this more clearly by rearranging:

$$\Delta T_s(t) = \frac{F - \epsilon N}{\lambda_{eq}}. \tag{2.3.12}$$

The discussion in the preceding sections can be summarized well using figure 2.2 from Yoshimori et al. (2016). The black crosses in the figure show the relation between ΔT_s and N under increasing CO_2 in a `1pctCO2` experiment. The TOA net radiation change increases approximately linearly with ΔT_s, with a slope given by κ, but it is important to note that κ decreases over time, at least in the CMIP5 models (Watanabe et al., 2013). The equilibrium climate sensitivity is estimated from an ensemble of `abrupt-4xCO2` experiments (blue crosses) using the method from Gregory (2004). Over the very long run the temperature change from constant forcing drifts slightly higher than the Gregory (2004) method predicts. Time variation in ϵ causes this drift; as the climate reaches equilibrium the heat uptake efficacy increases, meaning more surface temperature change is required to reach equilibrium.

Finally, we can follow Geoffroy et al. (2013*b*) in incorporating ϵ into the

two-box model, by adding it as a coefficient to H in equation (2.2.1):

$$C_s \frac{d\Delta T_s}{dt} = F - \lambda_s \Delta T_s - \epsilon H, \tag{2.3.13}$$

$$C_d \frac{d\Delta T_d}{dt} = H, \tag{2.3.14}$$

where H is defined as before. Below we briefly reproduce their results demonstrating the impact of different heat uptake efficacies on the shape of the $\Delta T - N$ curve. Previewing results from chapter 4, we can test the two-box model against a sample of data taken from the CMIP6 ensemble. Using estimates of C_s, C_d, and γ from Geoffroy et al. (2013*b*), it is straightforward to test the accuracy of equations (2.3.13) and (2.3.14) against the temperature change in `1pctCO2` runs. The results are shown in figure 2.3 for six of the models. These models use heat capacities $C_d = 100$ W yr m^{-2} K^{-1} and $C_s = 8$ W yr m^{-2} K^{-1}, and heat exchange efficiency $\gamma = 0.7$. The forcings $F(t)$ were calculated using the ERFs scaled linearly by the CO_2 emissions, the climate sensitivities λ_s from the Gregory (2004) method, and the heat sink from the surface was scaled using $\epsilon(\Delta T_s, N)$ averaged over the entire `1pctCO2` run. These three values were the only ones that varied; unlike in Geoffroy et al. (2013*b*) the heat capacities were not calculated independently and there was not a separate sensitivity assigned to the upper and deep ocean. Nevertheless, in four out of the six results the model predicts the shape of the transient response well, with $r > 0.98$ and $p \ll 1$ in all cases. On average, the toy model underpredicts the slope of the ΔT_s response by 4% for each of `ACCESS-CM2`, `CESM2`, `CESM2-WACCM`, and `CNRM-CM6-1`.

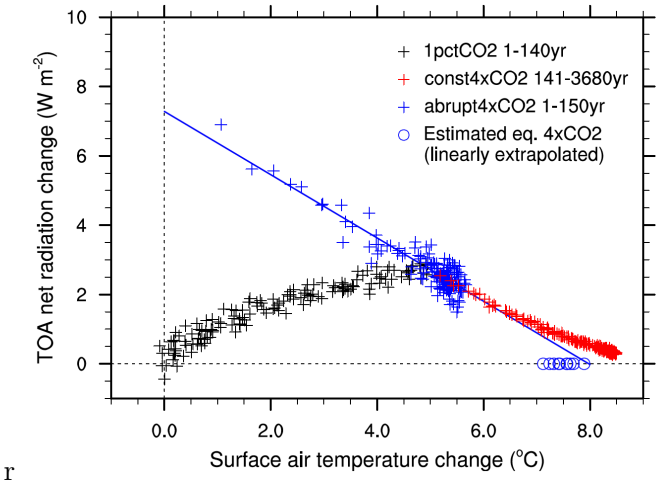

r

Figure 2.2: This figure, copied from Yoshimori et al. (2016), demonstrates the role of ocean heat uptake efficacy and efficiency. A higher efficacy in later years may explain the outwards sweep in ΔT_s which leads the Gregory (2004) method to underestimate the ECS.

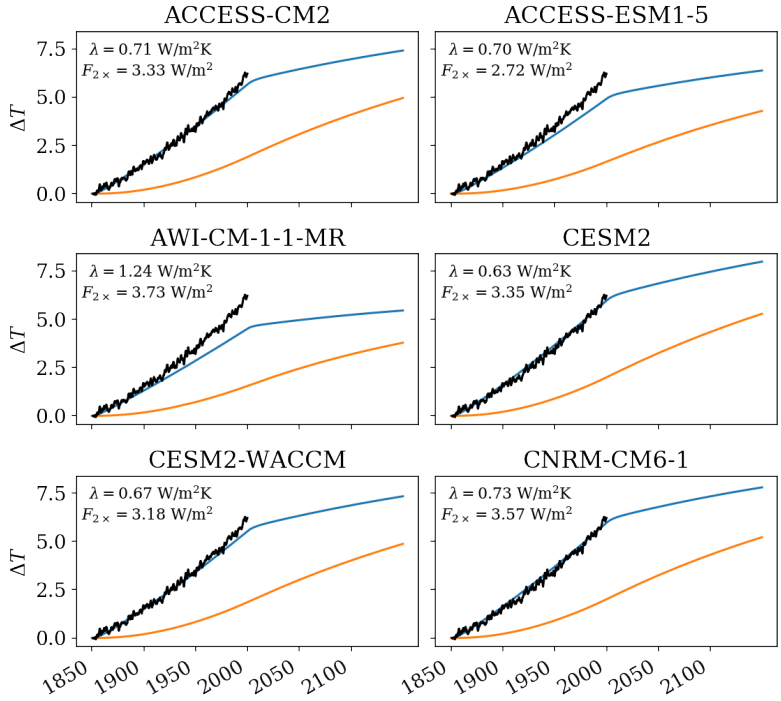

Figure 2.3: The two-box model in equations (2.2.1) and (2.2.2) fit to six members of the ensemble using $C_s, C_d = 8, 100$ W yr m^2 K^{-}1 and $\gamma = 0.7$, and the other parameters taken from the Gregory fits to the models.

Chapter 3

Mixed Layer Theory

GCMs in the CMIP5 ensemble tend not to simulate the surface mixed layer of the ocean very well (Huang et al., 2014). Based on the mixed layer depths in this study, the same could be said of the CMIP6 ensemble: these GCMs span a range of mixed layer depths, wider than the mean global average MLD over the ensemble; they also tend not to match observed depths (see Chapter 4). In other words, taken as a whole, they are neither accurate nor precise in calculating MLD. This result is not surprising. The depth of the mixed layer depends on turbulent processes (Langmuir circulation, shear and temperature instabilities, and breaking waves) that cannot be directly simulated in GCMs because their dynamics occur below grid scale (Thorpe, 2007). Accordingly GCMs have to parameterize these mixing processes. Parameterization of turbulent processes at grid scales is bound to be difficult, because the history of turbulence parameterization through methods such as second-moment closure shows that outside of large eddy simulations (LES), a good turbulence model is hard to find (Wyngaard, 2010).

3.1 Mixed layer turbulence

This section reviews the main turbulent processes which affect the MLD. Two important turbulent processes in the MLD concern heat and momentum fluxes. Following the discussion in chapters 2 and 3 of Thorpe (2007) we will describe how both of these fluxes contribute to the MLD and then describe the causes and effects of Langmuir circulation and turbulence.

In the absence of wind stress at the ocean surface, the main contributor to turbulence is the bouyancy flux, B. The bouyancy $b = g\delta\rho/\rho_0$, so B is defined as

$$B = \langle wb \rangle = \frac{g}{\rho_0}\langle w\delta\rho \rangle \tag{3.1.1}$$

where w is the vertical velocity. If we assume that changes in salinity are negligible over the region of interest we can relate B to the heat flux F_T as follows. First we note that

$$\rho \approx \rho_0(1 - \alpha T) = \rho_0 + \delta\rho$$

so long as $S \approx$ constant. Then we parameterize the heat flux by making the following assumption:

$$F_T = \langle \rho c_p w T' \rangle, \tag{3.1.2}$$

$$\approx -\rho c_p K_T \frac{dT'}{dz}. \tag{3.1.3}$$

Here T' is the local temperature deviation from the mean, c_p the heat capacity at constant pressure, and K_T is called the eddy diffusivity of heat, which in general can depend on z. Using the relation between $\delta\rho$ and T from above we find that

$$B = \frac{\alpha g}{c_p \rho} F_T. \tag{3.1.4}$$

A fluid particle gains potential energy as the product of its density variation and the rate at which it rises, in other words as $g\langle w\delta\rho \rangle = -\rho_0 B$. A gain in

potential energy implies a loss of turbulent kinetic energy (TKE) at a rate of $\rho_0 B$. If the temperature flux is constant then the bouyancy flux is divergence-less and the surface bouyancy flux B_0 roughly determines the turbulence.

Shear in the mean flow also produces turbulence (Thorpe, 2007). This term can be written as the product of the Reynolds stress $\tau = -\langle \rho w u \rangle$ and the mean shear, i.e.

$$F_S = -\tau \frac{dU}{dz}. \tag{3.1.5}$$

The Reynolds stress is often expressed in terms of the virtual *friction velocity* $u_* = \sqrt{\tau/\rho}$ or in other words $\tau = \rho u_*^2$. Based on a dimensional argument the shear can only depend on the distance from the surface, z, and u_*, so

$$\frac{dU}{dz} = \frac{u_*}{kz}, \text{ which means} \tag{3.1.6}$$

$$U(z) = \frac{u_*}{k}(\ln z - \ln z_0). \tag{3.1.7}$$

Here $k \approx 0.41$ is the empirical von Kármán's constant. This relationship, which holds near the boundary, allows estimation of the Reynold's stress and therefore the shear production of turbulence just from the horizontal velocity profile.

Langmuir turbulence is the last important source of ocean surface mixing covered here. Langmuir turbulence is a disordered form of Langmuir circulation (Li et al., 2019; Thorpe, 2004), which occurs when there is a Stokes drift: a net forward drift in a fluid in the presence of waves, caused by the fact that a circulating particle near the surface spends more time in the region below the crest of the wave, which is moving forward, and because velocity is greater near the surface (van den Bremer and Breivik, 2018). The second effect also means that the stokes drift $\boldsymbol{u}_{SD}$ has a strong vertical shear. This shear tilts the vertical vorticity which causes overturning circulation in the open ocean

surface boundary layer, in the plane perpendicular to the wind stress (Craik and Leibovich, 1976).

Early LES demonstrated that these Langmuir cells create turbulence. Two main methods for modelling that turbulence have arisen: K-profile parameterizations (KPP) and Langmuir turbulence production in second-moment closure models. In KPP schemes empirical relationships on different conditions are used to skip over the direct calculation of the TKE. For instance in the Langmuir case, the turbulent velocity scale is boosted by an enhancement factor which depends on the turbulent Langmuir number,

$$\mathrm{La}_t = \left(\frac{u_*}{u_{SD}} \right)^{1/2}. \tag{3.1.8}$$

La_t quantifies the ratio between wind-driven shear turbulence (represented by the friction velocity) and Langmuir turbulence. Different KPP approaches incorporate La_t into a boosting coefficient of varying forms.

Second-moment closure models handle TKE by parameterizing all of the terms in its equation. These models have been used to try to incorporate Langmuir turbulence into ocean models (van den Bremer and Breivik, 2018). For instance, one approach adds a term proportional to the shear of $\boldsymbol{u}_{SD}$ to the TKE equation (Kantha and Anne Clayson, 2004).

Langmuir turbulence is an important mixing scheme for the global climate system, but was not represented explicitly in CMIP5 models, which may have contributed to their persistent MLD biases (which cannot be explained by surface forcing: Li et al. (2016); Huang et al. (2014)).

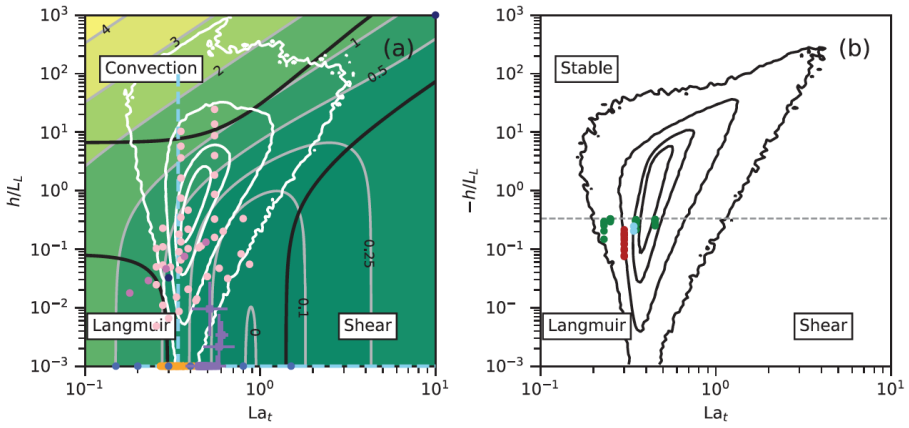

Figure 3.1: A copy of Figure 1 taken from Li et al. (2019). The left panel (a) reproduces the figure from Belcher et al. (2012), which illustrates which turbulence schemes dominate depending on the values of La_t and h/L_L, with destabilizing buoyancy flux (thick black line = greater than 90% contribution). The white lines indicate the 2-dimensional pdf of all of the JRA55-do forced simulations for which buoyancy production was positive (about 62% of instances). Background filled contours correspond to the normalized turbulent dissipation rate. Note that none of the simulations enter the high-shear-production region. Panel (b) plots the equivalent pdf but for stabilizing buoyancy flux (the remaining 38% of instances). Dots indicate the regimes used in LES studies; since we are not as concerned about these the legend is omitted from this copy.

3.2 Langmuir turbulence parameterizations and MLD

As one important example of the modeling decisions which can affect MLD, this section reviews the main findings by Li et al. (2019), who investigated the impacts of different Langmuir turbulence parameterizations on MLD under various forcing schemes. Six different Langmuir turbulence parameterizations (henceforth LT, following Li et al.) are considered and their resulting MLDs and stratifications are compared to five non-LT counterparts. The LT parameterizations include both KPP and second-moment closure models. They modify a common *turbulence diffusion* scheme which is similar in form to the

expression for F_T in the previous section:

$$\overline{w'\lambda'} = -K_\lambda \partial_z \overline{\lambda} + \Gamma_\lambda, \text{ where} \tag{3.2.1}$$

$$K_\lambda = C_\lambda q l. \tag{3.2.2}$$

Here λ is an arbitrary quantity; $K_\lambda > 0$ is the eddy diffusivity which depends on a velocity scale q, length scale l, and nondimensional coefficient C_λ (all of which may vary with z); and Γ_λ represents any fluxes not proportional to the local λ-gradient. The six different LT parameterizations modify equation 3.2.1 under different assumptions and using variants of the Langmuir number La_t. Specifically, they do one or more of the following: (1) boost K_λ by increasing one of its components; (2) modify the vertical profile of K_λ to account for the structure of Langmuir circulation; (3) modify Γ_λ, which generally depends on coherent structures in the boundary layer, of which Langmuir cells are one such structure; (4) include a down-Stokes drift shear momentum flux, which is also treated as "nonlocal"; (5) include a momentum flux in a direction different than the shear orientation, because LES simulations show that the turbulent momentum flux is often misaligned from the shear; (6) enhanced entrainment at the base of the surface boundary layer due to unresolved shear, because plumes generated by Langmuir turbulence increase entrainment; and (7) enhanced entrainment from resolved shear, in which Langmuir circulation reduces surface shear and increases shear at the base of the boundary layer.

Li et al. use three classes of initializations and surface forcings to assess the different schemes. The first is a simulation with forcings taken from ocean station data at three different locations and over different time periods, in order to simulate wintertime MLD deepening, springtime shoaling, and a full year cycle. The second test case uses a global forcing from the JRA55-do dataset. The ocean is gridded into a set of $4^\circ \times 4^\circ$ one-dimensional models, and

each model is evaluated over a full year using the forcings and initializations at each grid point. Since Li et al. only test one-dimensional parameterizations which ignore important lateral mixing and transport phenomena, they cannot meaningfully compare the output to real observations in these first two test cases. Instead the MLDs resulting from the different test cases are compared within the ensemble. In the second test case the models are re-initialized each month to match the forcing and profile dataset so that the drift away from the expected values does not become too large, while still giving time for the models to diverge from each other due to intrinsic variability.

The third test case compares the 11 models to two LES, and they are initialized and forced using the same values applied to the LES. These are meant to simulate, first, a case with constant wind, waves, and destabilizing surface bouyancy flux ($B_0 < 0$). The second simulates transient hurricane-force winds. Here some meaningful comparisons between the LES and the (non) LT parameterizations can be made and, the authors hope, used to explain variability in the other two test cases.

We will now quickly summarize the results from each test. The results from test 1 showed that LT and non-LT schemes all generated significantly different results with overlap between the two groups in both MLD and bouyancy. However the LT parameterizations tended to give more rapid deepening of the MLD under destabilizing surface conditions.

The results from test 2 demonstrated that LT and non-LT parameterizations had large differences in MLD regionally and on a global scale. (Due to the monthly reinitialization these likely underestimated the actual differences.) The LT parameterizations predicted a $6\%[-2\% - 14\%]$ deeper MLD on average than their non-LT counterparts. Figure 3.1 is a copy of Figure 1 from Li et al. It shows the parameter space spanned by all of the JRA55-

do forced tests, defined with regards to La_t and the parameter h/L_L, which measures the relative important of convection versus Langmuir turbulence. Here h is a representative depth scale for the mixed layer (e.g. MLD) and $L_L = -u_*^2 u_{SD}/B_0$ is the Langmuir stability length. According to Li et al., most of the ocean is either dominated by Langmuir turbulence (i.e. small La_t and small h/L_L, or by a mixture of Langmuir and buoyancy turbulence.

Importantly, large areas of the Southern Ocean are dominated by Langmuir turbulence. The LT parameterizations also show systematically deeper MLD in these regions than the reference. As we will see, within the 16-member ensemble used here there are large inter-model variations in Southern Ocean MLD: up to 80% of the inter-model mean MLD, and larger than anywhere else except a thin band at northern latitudes. Together these observations leave open the possibility that variations in surface layer turbulence parameterizations, and particularly Langmuir turbulence, could explain some of the differences in MLD between models in the ensemble.

There is one result from the third test case of interest for this study. All non-LT parameterizations significantly underpredicted the entrainment at the bottom of the surface boundary layer in Langmuir turbulence schemes as compared to the LES. This result could indicate that differences in LT parameterization affect the depth and height of the thermocline. In the next chapter we will see that thermocline ventilation may be important for explaining the results.

What can we conclude from Li et al.? We want to explain inter-model variations in global average mixed layer depth of 20-30 meters. On average the LT parameterizations in the global test case were less than 5 m deeper than their counterparts over the entire globe. This result makes it appear unlikely that Langmuir turbulence parameterizations alone could explain the MLD spread

in CMIP6. Additionally the LT schemes predict a deeper MLD especially when convection is weak, as in the Southern Ocean during austral summer; but in the CMIP6 ensemble most of the MLD spread during those months is confined to the Northern latitudes. However, the authors do note that the global simulation likely underestimates the divergences between models because of monthly reinitialization. Additionally, the results from tests 1 and particularly 3 indicate that different LT parameterizations may significantly impact entrainment at the bottom of the boundary layer and bouyancy production. These processes could provide a coupling to the thermocline and lead to the $\epsilon - h$ correlation referred to in the introduction. In summary, it appears that characterizing the mixed layer turbulence parameterizations in the CMIP6 set along the same lines used in Li et al. (2019) would at least indicate whether there are systematic differences in MLD according to the parameterizations, and in this case we have reason to dig deeper into the particular effects of LT parameterizations.

3.3 Frankignoul and Hasselmann's MLD feedback

Having reviewed the main processes contributing to mixed layer turbulence, and one explanation for intermodel variability in MLD, we now turn to the last piece motivating the hypothesis stated in the introduction: that variability in MLD might explain variability in climate sensitivity, according to the relation in equation 1.0.1, which is:

$$\frac{dT_{os}}{dt} = \frac{F_o}{c_s h} - \lambda_o T_{os}.$$

Equation 1.0.1 is a simple hypothetical linear feedback describing an interaction between the oceanic mixed layer and atmospheric temperature, similar in form to equation 2.1.16. This model was first proposed in Frankignoul

and Hasselmann (1977). We will briefly review the context in which it was proposed and the conceptual leaps required to apply it to the globe as a whole.

Hasselmann (1976) describes mechanisms by which internal weather variability in climate models can explain *climatic* variability. Hasselman argues that the larger climate system can be seen as an integrator of small-scale weather variability. Whereas previous low-dimensional nonlinear models of weather or climate were deterministic — all variability was ascribed to boundary conditions — Hasselman argues that internal time-dependent variability on the scale of the climate system can arise due to stochastic changes at a much smaller scale. As opposed to real turbulent systems, in which TKE transfer occurs across a wide spectrum of length scales, Hasselman stipulates that there are two strongly separated timescales of motion for the smaller, stochastic weather processes and the climatic ones. Formally, the weather and climate systems are divided into vectors of variables $\mathbf{x}$ and $\mathbf{y}$, and related through:

$$\frac{dx_i}{dt} = u_i(\mathbf{x}, \mathbf{y}) \tag{3.3.1}$$

$$\frac{dy_i}{dt} = v_i(\mathbf{x}, \mathbf{y}), \tag{3.3.2}$$

where the timescale of y is much larger than the timescale of change in x. Treating $\mathbf{x}$ as a stationary random variable, for small excursions away from a mean value $\rangle \delta y \langle$, the deviation in y_i from the mean value — in other words the evolution of the fluctuating term y_i' in y_i — can be described as

$$\frac{dy_i'}{dt} = v_i(\mathbf{x}, \mathbf{y}) - \langle v_i \rangle = v_i'. \tag{3.3.3}$$

Integrating over time, the stochastic changes in x entail that the fluctuating term in y_i is non-stationary, and the covariance matrix $\langle y_i' y_j' \rangle$ grows linearly. The climate system takes on greater variability from the mean state as it integrates variability in the weather system. By way of analogy, we can see

the climate system as a collection of Brownian particles, in which smaller particles (weather systems) over time collide with larger particles and increase their average variation.

Real climate variability does not grow indefinitely, and Hasselmann (1976) argues that this is because on longer timescales ($t \approx \tau_y$) stabilizing feedbacks dampen the effect of integrating weather variability. In Frankignoul and Hasselmann (1977), the authors propose one such feedback between slowly-changing mixed layer temperatures and rapidly fluctuating atmospheric temperatures. Formally, they write the time evolution of the heat content of the mixed layer as

$$h\frac{dT_o}{dt} = \frac{H_s + H_L}{\rho^w C_p^w}, \tag{3.3.4}$$

where H_s is the sensible heat flux at the surface of the mixed layer, H_L is the latent heat flux, and ρ^w and C_p^w are the density and specific heat, respectively. This simple model assumes a constant mixed layer depth and no radiative heat flux or heat loss to the deep ocean from the mixed layer. This equation can be reformulated to account for fluctuations ΔT_o about a mean T_o caused by deviations of f_1 from the equilibrium value $[f_1]$ (here I write those deviations as F_o). Using $\lambda_o = (\partial[f_1]/\partial\Delta T_o)_{\Delta T_o=0}$, they write:

$$\frac{dT_{os}}{dt} = \frac{F_o}{c_s h} - \lambda_o T_{os}, \tag{3.3.5}$$

which is the same as equation 1.0.1. This equation is identical in form to the energy balance in equation 2.1.16, except that here λ has an apparent dependent on h.

This similarity motivates the original hypothesis of this thesis, which is that intermodel differences in MLD might contribute to different climate sensitivities. For this hypothesis to be feasible we need to make a number of conceptual jumps. First, while λ_o has an h-dependence which we exploit to

formulate the hypothesis, that h-dependence only acts *between* different models with constant mixed layer depths. If we drop the assumption of constant h *within* models, the above equation no longer holds true, and we have to deal with the original nonlinear form for $d(hT)/dt$. However we know that h is in fact *never* constant, so to assume that this model could still hold approximately correct the variations in T need to dominate the variations in h. Second, the hypothesis ignores time and spatial variation in feedbacks, despite evidence indicating their importance (Armour et al., 2013). Third, the hypothesis assumes that we can treat local changes to ocean surface temperatures as equivalent to (or tightly linked with) global changes in surface temperature. Acknowledging these large assumptions, we now turn to evidence from the CMIP6 ensemble.

Chapter 4

Results: mixed layer depth and climate sensitivity

Having established a motivating conceptual model of the climate system (chapter 2) and discussed some reasons for variation and uncertainty in mixed layer parameterizations of climate models (chapter 3) we now turn to the actual data. This chapter uses an ensemble of sixteen models from the CMIP6 ensemble (Eyring et al., 2016). The goal of is to investigate whether there are significant and systematic relationships between variation in mixed layer depth and variables affecting climate sensitivity between the members of the ensemble. To answer this question we look at a number of correlations between outputs from the different models. I emphasize that due to the nature of this study it is impossible to establish the existence of causal mechanisms in any of the cases discussed. No climate model parameters were tuned and no new output was collected in the writing of this thesis. The best we can do is detect interesting and strong correlations which might point to useful experiments or questions for further study.

The first question we ought to ask about these models is whether there are

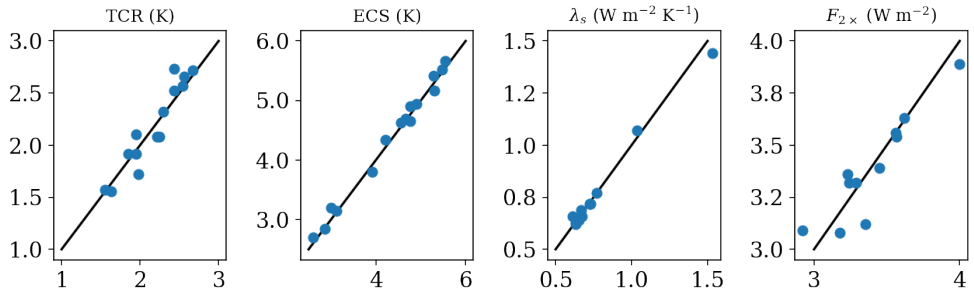

Figure 4.1: Values for the variables calculated here (x axis) versus the published values in Nijsse et al. (2020) (y axis). The black line indicates a 1:1 relation. TCR was calculated as the mean temperature change from the preindustrial control between years 61-80 in `1pctCO2`; the remaining three variables were calculated following Gregory (2004).

any interesting inter-model differences in the first place. Within the ensemble, the surface temperature equilibrium climate sensitivities calculated here using the methods from Gregory (2004) vary between 2.61 K and 5.54 K, in good agreement with other published values (figure 4.3; the most recent published values are collected from Nijsse et al. (2020)). The TCRs vary between 1.56 K and 2.67 K. These results corroborate the high variation and upwards bias in climate sensitivities that have been reported for past and present CMIP ensembles (Flato et al., 2013; Nijsse et al., 2020).

In addition to significant variability in climate sensitivities, there are large global and region differences in mixed layer depth between the members of this ensemble. Figure 4.2 (right) shows the 10-year moving global average mixed layer depth (h) for all members of the ensemble over 150 years of a `1pctCO2` run. The two outliers (AWI-CM-1-1-MR and NESM3) range between $h \approx 20$ m and $h \approx 100$ m. Even excluding these two, the average depths in the center of the range span a range from 40 m to 80 m.

It is also clear from the top right panel of figure 4.2 that the global average mixed layer depth decreases over time. There are two things to note. First,

the ordering of the ensemble by h remains nearly constant over the course of the run, meaning h decreases at nearly the same rate across the different models despite large differences in starting h. Across the ensemble, the global average of h at any time $t \in [0, 150]$ years remains correlated to the average of h over the first ten years with $p \ll 0.05$ and $r > 0.98$ for `abrupt-4xCO2`, `1pctCO2`, and `piControl` experiments (see Appendix 1).

One of the first questions we must ask is: does the assumption of constant mixed layer depth implicit in equation (1.0.1) and the treatment of the two-box model (2.2.1) hold approximately true? The top left panel in figure 4.2 shows the change in global average surface temperature change $\Delta T_s(t)$ divided by the average change over the entire run ($\overline{T_s}$ in the legend) as the dashed lines, and the analogous calculation for the mixed layer depth as the solid lines. Whereas ΔT increases from zero to double its mean value, the decreases in mixed layer depth in no case amount to more than 50% its average value. This result gives reason to trust the constant-h assumption, although not fully conclusive evidence that the nonlinearity in equation (2.2.1) can be ignored.

4.1 Global mixed layer depth

Having established the validity of some basic assumptions, there are three preliminary questions we might ask:

1. Does the ECS vary in proportion to the TCR?

2. Does the two-box model from chapter 2 predict the response to `abrupt-4xCO2`?

3. Does the global average mixed layer depth correlate to ECS, TCR, or any of the other measures of climate response introduced in chapter 2?

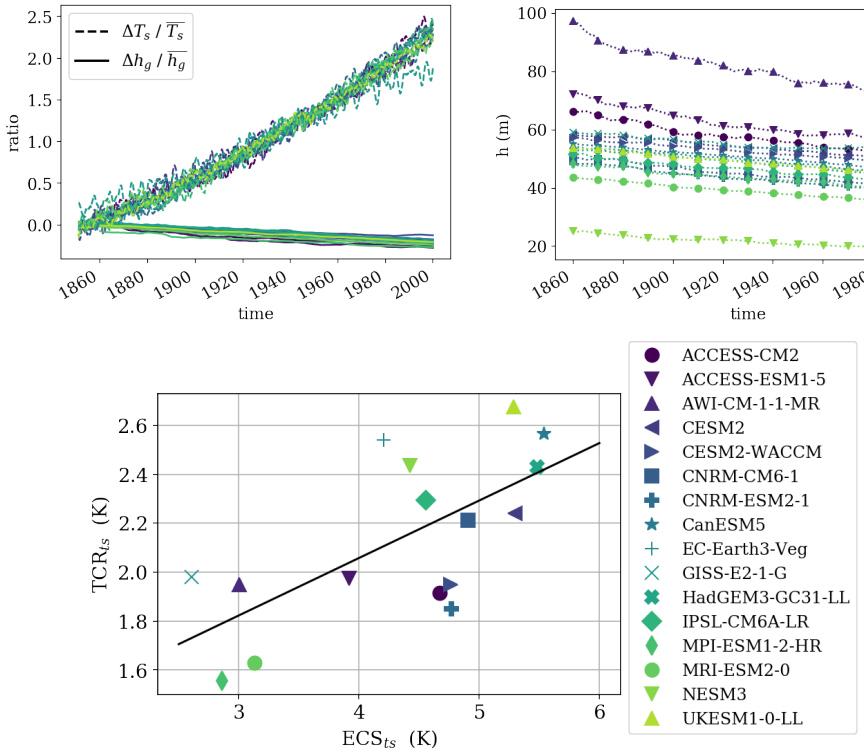

Figure 4.2: Checking some basic assumptions. **Top right**: The ratio of $\Delta T_s(t)$ (dashed lines) and $h^g(t)$ (solid lines) to their time averages throughout the ensemble. **Top left** the 10-year moving average h^g for the `1pctCO2` ensemble. **Bottom** The relationship between TCR and ECS for the 16 models used in this ensemble. TCR is calculated as the average of ΔT_s from 61-80 years and ECS as $1/2$ the $N = 0$ intercept of the Gregory diagram.

The first question can be answered straightforwardly: as we would expect, there is a correlation between the equilibrium and transient climate sensitivities. Linear regression of the ECS against the TCR (defined with respect to surface temperature `ts`) yields slope $= 0.235$, $r = 0.675$, and $p = 0.004$. The same regression but carried out using variables defined with respect to ocean surface temperature (`tos`) gives slope $= 0.259$, $r = 0.593$, and $p = 0.015$.

The second question can be answered to varying levels of accuracy. First we can plot the measured ΔT_s from the `abrupt-4xCO2` ensemble against the calculated values using the two-box model with ϵ from equations (2.3.13)-

(2.3.14). The results for the two `ACCESS` models are displayed in Appendix B, figure B.1. The values of ϵ used in these calculations were taken as the time-average of ϵ calculated over the last thirty years of the `1pctCO2` runs, during which ϵ shows greatest convergence.[1] As can be seen, in neither case does the linear model fit the data very well qualitatively. One possible explanation for this is that the transient response used to calculate ϵ does not give enough information to do so accurately.

Finally, we might ask whether the mixed layer depth correlates with either measure of climate sensitivity. Recall from chapter 3 that the Frankignoul and Hasselmann (1977) theory predicts an inverse relationship between h and ΔT. However we know in advance that this theory is a large oversimplification, especially when applied to the globe and extrapolated to surface temperatures and TOA forcing. (The original theory applies only to the local temperature and forcing *at the mixed layer*.)

The immediate answer appears to be: no. Figure A.6 plots the correlations between the global mixed layer depth h^g at time t and eight other variables (for more information, see Appendix A). A significant ($p < 0.05$) correlation is below the solid red bar at the bottom of the plots. As we can see from figure A.6, the global average mixed layer depth does not significantly correlate with either the global surface or ocean surface temperature at any time throughout the course of the `1pctCO2` runs. Neither does it correlate significantly with any of the other variables assessed at any time. By itself this is a significant result. There are a number of possible explanations. For instance, variations in the mixed layer depth between models may not affect the rate or magnitude of temperature change because the mixed layer did not correlate positively to the depth of the surface box in the two-box model. However, we now turn to

[1] This calculation scales the ECS in the numerator by the year, so that $\Delta_{eq} = ECS \times t/70$.

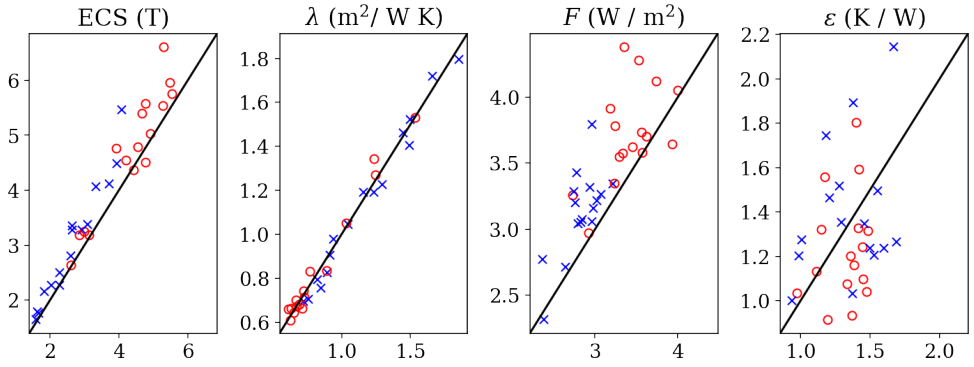

Figure 4.3: Values for the variables calculated following Gregory (2004) (x axis) versus those calculated following Geoffroy et al. (2013*a*) (y axis). The black line indicates a 1:1 relation. The red circles are calculated using the global surface temperature, and the blue crosses using the SST.

the more surprising results found after applying the model of Geoffroy et al. (2013*b*,*a*).

4.2 An inverse relationship between the mixed layer and the active layer

Geoffroy et al. (2013*b*) calculate ϵ using a multilinear regression of N against F, λ, ϵ, and H, and additionally calculate C_s, C_d, and γ. This method is described in greater depth in Appendix B. The resulting fits include revised estimates of λ and F, and are much closer to the model output. They allow us to calculate ϵ directly using just the `abrupt-4xCO2` run. In the simple model used previously, no distinction is made between ocean surface and atmospheric temperatures and further the values of C_d, C_s, and γ are taken simply as the average from Geoffroy et al. (2013*b*).

The surface layer in this two-box model is easily associated with the mixed layer; both have a similar size (the heat capacity of the surface layer equals that of the top ∼100 m of ocean), and there is reason to think that the mixed

layer influences the short-term response to warming similarly to the surface layer. Counter-intuitively, there is in fact a statistically significant *negative* correlation between the global average mixed layer depth, taken over the first ten years of the run, and the surface-layer depth in the two-box calculation, $h_s = C_s/\rho c_p$. The correlation coefficient is $r = -0.74$ and $p = 0.002$.[2] We use the average MLD over the first ten years because h tends to decrease significantly decades into the run. In other words, the surface box in the two-box model is sometimes interpreted as akin to the mixed layer (Geoffroy et al., 2013*b*), but this appears to be the opposite of the truth, despite the two being of similar magnitude. To make a clearer distinction between these two quantities throughout, we will refer to the surface layer in the two-box model as the *active layer*.

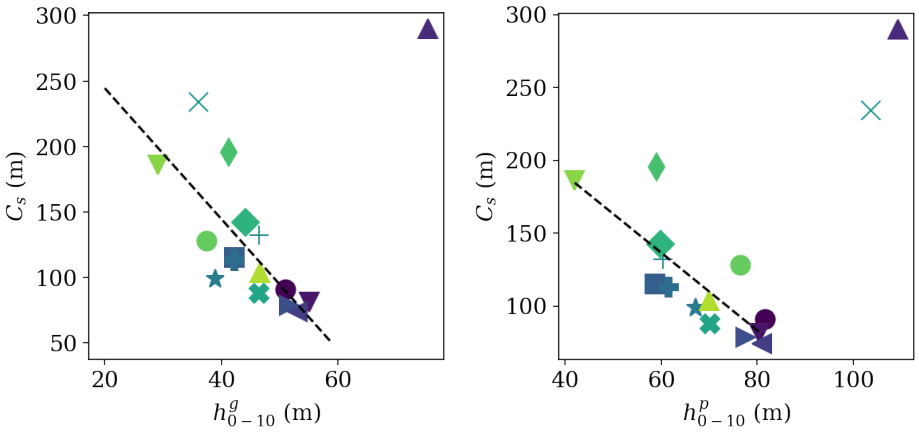

Figure 4.4: **Right**: The two-box C_s plotted against the global average mixed layer depth over the first ten years of `abrupt-4xCO2`, h^g_{0-10}. With `AWI-CM-1-1-MR` excluded the fit has $r = -0.74$ and $p = 0.002$. **Left**: The same plot but with the subpolar average MLD, h^p_{0-10}. With `AWI-CM-1-1-MR` and `GISS-E2-1-G` excluded the fit to the subpolar MLD, h^p_{0-10}, has $r = -0.80$ and $p = 0.0006$.

[2]Note however that this correlation only holds if the model `AWI-CM-1-1-MR` is excluded from the fit. From here forward `AWI-CM-1-1-MR` is excluded from all correlations unless explicitly stated. This model has an anomalously deep mixed layer near the South Pole and high wind stresses compared to every other member of the ensemble.

The previous point does not by itself explain the lack of a significant correlation between mixed layer depth and temperature change – in fact, it gives reason to expect a significant *positive* relationship, which we do not see in the plotted `1pctCO2` correlations in Appendix A. The variations in global mixed layer depth between runs may not have this correlation in part because the surface layer response time is too short for them to matter much. The average short response time $\tau_s = 10.8$ yr, whereas significant temperature differences between step-forcing experiments may emerge well beyond this point.

Critically, the correlations in Appendix A do not take into account the corrections to F, λ, and the ECS that emerge from the two-box calculations. Once we take these into account, there emerges a moderate correlation between the ECS and h^g_{0-10}, with $r = 0.58$ and $p = 0.022$. Additionally, the calculated ϵ values correlate strongly with h^g, with $(r, p) = (0.82, 0.002)$. A full set of correlations between variables calculated using the EBM-ϵ model with both global surface temperature and SST are displayed in tables 4.1 and 4.2.

4.3 Explaining the MLD correlations

The previous results suggest that the original hypothesis of this thesis is incorrect, and they point to a relationship between the mixed layer and the active layer that is the inverse of that originally expected. By itself, the fact that the original hypothesis was not supported is not surprising. Gregory (2000), in the original paper proposing the two-box model, pointed out that the active layer should not be identified with the mixed layer. However, the strong *negative* correlations between mixed layer depth and active layer size indicate that there may be a mechanistic relationship underpinning differences in the short timescale response. Additionally, the ECS correlates significantly with C_s and with h under certain circumstances (see table 4.1), indicating the potential to

	h^p_{0-10}	h^g_{0-10}	C_s	C_d	λ	$F_{2\times}$	ϵ	ECS_{ts}	$\mathrm{ECS}^{(1)}_{ts}$	TCR_{ts}
h^p_{0-10}	-	**0.79**	**-0.80**	**0.54**	-0.29	0.06	**0.67**	0.39	0.10	-0.27
h^g_{0-10}		-	**-0.74**	0.37	-0.49	0.07	**0.82**	**0.58**	0.34	-0.03
C_s			-	0.03	**0.87**	0.26	-0.51	**-0.83**	**-0.73**	-0.21
C_d				-	0.35	0.34	0.50	-0.14	-0.38	**-0.63**
λ					-	0.41	-0.21	**-0.87**	**-0.90**	-0.49
$F_{2\times}$						-	0.48	0.06	-0.13	0.06
ϵ							-	0.45	0.12	-0.12
ECS_{ts}								-	**0.93**	**0.57**
$\mathrm{ECS}^{(1)}_{ts}$									-	**0.67**
TCR_{ts}										-

Table 4.1: Two-box ϵ correlations, T_s = `ts`. This table displays r-correlations between the variables obtained by application of the EBM-ϵ model from Geoffroy et al. (2013*a*), using `ts` as the surface temperature. Numbers in **bold** have $p < 0.05$ using a two-sided Wald Test for linear correspondence. h^g_{0-10} corresponds to the global average MLD over the first ten years and h^p_{0-10} to the subpolar average MLD. The superscript $^{(1)}$ indicates values calculated using the method from Gregory (2004). `AWI-CM-1-1-MR` was excluded from all correlations and `GISS-E2-1-G` was excluded from the $h^p_{0_10}$ correlations.

	h^p_{0-10}	h^g_{0-10}	C_s	C_d	λ	$F_{2\times}$	ϵ	ECS_{tos}	$\mathrm{ECS}^{(1)}_{tos}$	TCR_{tos}
h^p_{0-10}	-	**0.79**	**-0.64**	-0.15	-0.45	**0.56**	**0.68**	**0.60**	0.50	0.12
h^g_{0-10}		-	**-0.86**	-0.37	**-0.78**	0.48	**0.79**	**0.78**	**0.71**	0.31
C_s			-	**0.54**	**0.96**	-0.34	**-0.62**	**-0.93**	**-0.91**	**-0.54**
C_d				-	**0.63**	-0.26	-0.11	**-0.60**	**-0.70**	**-0.65**
λ					-	-0.24	-0.46	**-0.90**	**-0.92**	**-0.58**
$F_{2\times}$						-	**0.65**	**0.57**	0.50	0.31
ϵ							-	**0.65**	0.48	0.10
ECS_{tos}								-	**0.97**	**0.54**
$\mathrm{ECS}^{(1)}_{tos}$									-	**0.63**
TCR_{tos}										-

Table 4.2: Two-box ϵ correlations, T_s = `tos`. The table shows r correlation coefficients between variables as above, but all values calculated from the two-box ΔT fit using `tos` as the surface temperature. Numbers in **bold** have $p < 0.05$ using a two-sided Wald Test for linear correspondence.

develop an emergent constraint on ECS if the relationship to MLD can be understood.

One path towards understanding this relationship involves the regional

variations in MLD. The MLD varies significantly both over time and with latitude. In the subpolar regions (loosely defined here as $|lat| < 50°$), h can reach several hundreds of meters, while near the equator it often remains in the 20-70 m range. Figure 4.5 shows these differences: each plot shows the latitudinal band averages of h (color, vertical by latitude) against time (horizontal axis), with darker colors representing deeper MLDs. We observe that there are large differences between model MLD in the subpolar regions, and that these differences partially fade with time as the ML in the higher latitudes shallows.

Boé et al. (2009) found that the mixed layer depth at high latitudes ($> 58°$ N and $> 68°$ S) correlated significantly with a decreased transient climate response. They conjectured, following Winton et al. (2010), that the subpolar mixed layer depth may increase the ocean heat uptake efficacy and therefore the difference between TCR and ECS. This may occur because a deeper mixed layer near the poles leads to more effective mixing of warm surface water into cool deep ocean overturning cells. However, the correlations between MLD and ECS were found to be stronger using *global* mixed layer depth than with the subpolar mixed layer depth, however, which casts some ambiguity on the conjectural relation based in Boé et al. (2009).

One natural hypothesis is that the active layer in the EBM-ϵ model is actually the thermocline, and that models with a greater C_s are those in which the thermocline is ventilated more effectively. The size of the thermocline approximately matches C_s. The theory of thermocline ventilation is beyond the scope of this thesis (see Vallis (2017, Ch. 20) for an overview), but we note that the height of the thermocline scales with surface wind forcing. A preliminary check found that, for the thirteen models for which zonal wind stress could be downloaded, there was a significant correlation between the

average global wind stress and the size of the active layer, lending credence to this theory. Further study should look into whether ensemble differences in the change in potential temperature within the thermocline support the hypothesis that the heat in the active layer ends up in this region of the ocean.

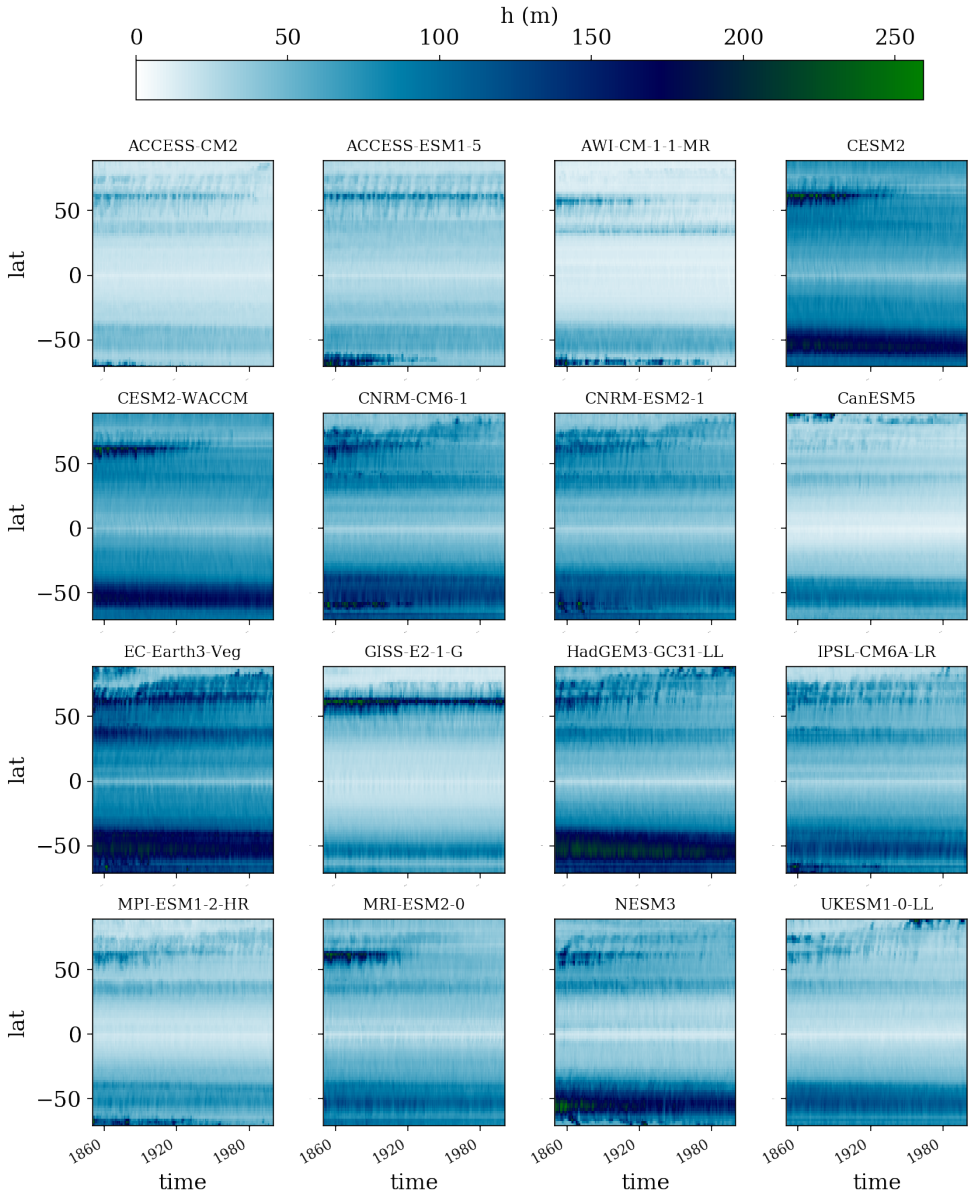

Figure 4.5: Twelve-month rolling average mixed layer depth by latitude over the 16-member ensemble, over the course of a `1pctCO2` run up to $4\times CO_2$. Due to the distribution of mixed layer depth h, the subpolar mixed layer depth h^p for latitudes greater than 50° N and S was defined as an important variable for correlation. The mixed layer depth at northern latitudes decreases with time consistently across the ensemble, and the latitude of deepest mixed layer moves further north over time.

Chapter 5

Conclusions

This thesis began with the hypothesis that greater mixed layer depth implies slower transient response to warming in climate models. Chapter 2 developed a simple conceptual model of climate change and global warming time scales, and Chapter 3 reviewed the turbulent processes that contribute to mixed layer depth and the reasons for thinking that models with greater MLD might warm less. Chapter 4 then found that no such correlation exists. After applying the slightly more complex EBM-ϵ model developed in Geoffroy et al. (2013*b*), it was seen that a deeper MLD correlates negatively with the size of the active layer, which determines the short-term response to forcing. This counterintuitive result not only disproves the original hypothesis (at least within this ensemble of models); it also indicates that the strong negative correlation between MLD and C_s might be used to identify the active layer in the EBM$-\epsilon$ model.

The possibility of an emergent constraint

The striking correlation between global average mixed layer depth and the recalculated ECS begs the further question: could MLD impose an emergent

constraint on equilibrium sensitivity? If so, comparisons of observations by the Argo (Argo, 2020) network to climate models could significantly constrain the equilibrium climate sensitivity, along the lines of Boé et al. (2009) and analagous to Nijsse et al. (2020). It may be very difficult to do this well, however, without knowing, first, *why* MLD varies between models and, second, which mechanisms relate to the postulated causal structure.It still remains to be seen whether a causal mechanism linking MLD to the equilibrium response behaves accurately within these models. Even if it did, it is not entirely clear that the ECS and ϵ calculated via Geoffroy et al. (2013*a*) are superior to those calculated through the simpler model, although the results in appendix B indicate that the EBM$-\epsilon$ theory fits most of the models well.

Finally, I conjectured that the active layer in the EBM$-\epsilon$ model may be the thermocline. In this case differences in thermocline ventilation may explain the different heat uptake efficacies and depths of the active layer. However, we would then need to explain why thermocline ventilation correlates negatively with mixed layer depth. A preliminary check showed that zonal wind stress does correlate significantly with active layer depth across a subset of these models. Since zonal wind stress also forces thermocline depth, this is *prima facie* evidence in favor of this explanation. Further investigation is needed — in particular, vertical profiles of potential temperature should be used to assess whether the heat absorbed by the active layer does in fact end up in the thermocline. If this causal mechanism can be shown and its relation to mixed layer depth is robust, then there will be potential for an emergent constraint based on mixed layer depth in the CMIP ensemble.

Appendix A

Inter-ensemble MLD Correlations

This section shows the inter-ensemble correlations plotted between various measures of the mixed layer depth and a set of eight climate variables defined by reference to the two-box model. The measures of mixed layer depth in this section use the following convention: $\overline{h_{0-10}}$ means that the measure was taken as the average over the first ten years and that constant value was correlated to the other variables over time. Δ means that the difference $h(t) - \overline{h(0-10)}$ was correlated to the global mean of each variable at each time t. If neither of the preceding qualifications apply, $h(t)$ was correlated directly with the given variables. The superscripts h^g and h^p correspond to global and subpolar ($|lat| > 50°$) weighted averages, respectively.

All of these figures correspond only to `1pctCO2`, not `abrupt-4xCO2`, although some of the variables calculated here rely on both. The variables correlated with h are: N, the net TOA downwards heat flux per m^2 over the globe; Q, the net global heat flux into the ocean surface per m^2; κ, the heat uptake efficiency or slope of the $N - T$ relation; C_{eff}, the effective heat

capacity, which gives a rough gauge of how much of the ocean is engaged in the climate system at a given time; ΔT_s, the change in surface temperature compared to preindustrial; ΔT_{os}, the change in ocean surface temperature compared to preindustrial; ϵ, the ocean heat uptake efficacy, calculated using $\Delta T_{eq} = ECS \times F(t)/F_{2\times}$; and h_g, the global average MLD at time (t) — which shows whether, for instance, the starting variations in subpolar MLD can predict future variation in global average MLD (they can).

The inter-ensemble correlations were calculated by linearly regressing the two variables at each 10-year timestep, taking a 20-year average about t. The regression function used was `scipy`'s `linregress()`, which calculates the p value using a two-sided Wald Test with a t-distribution of the test statistic.

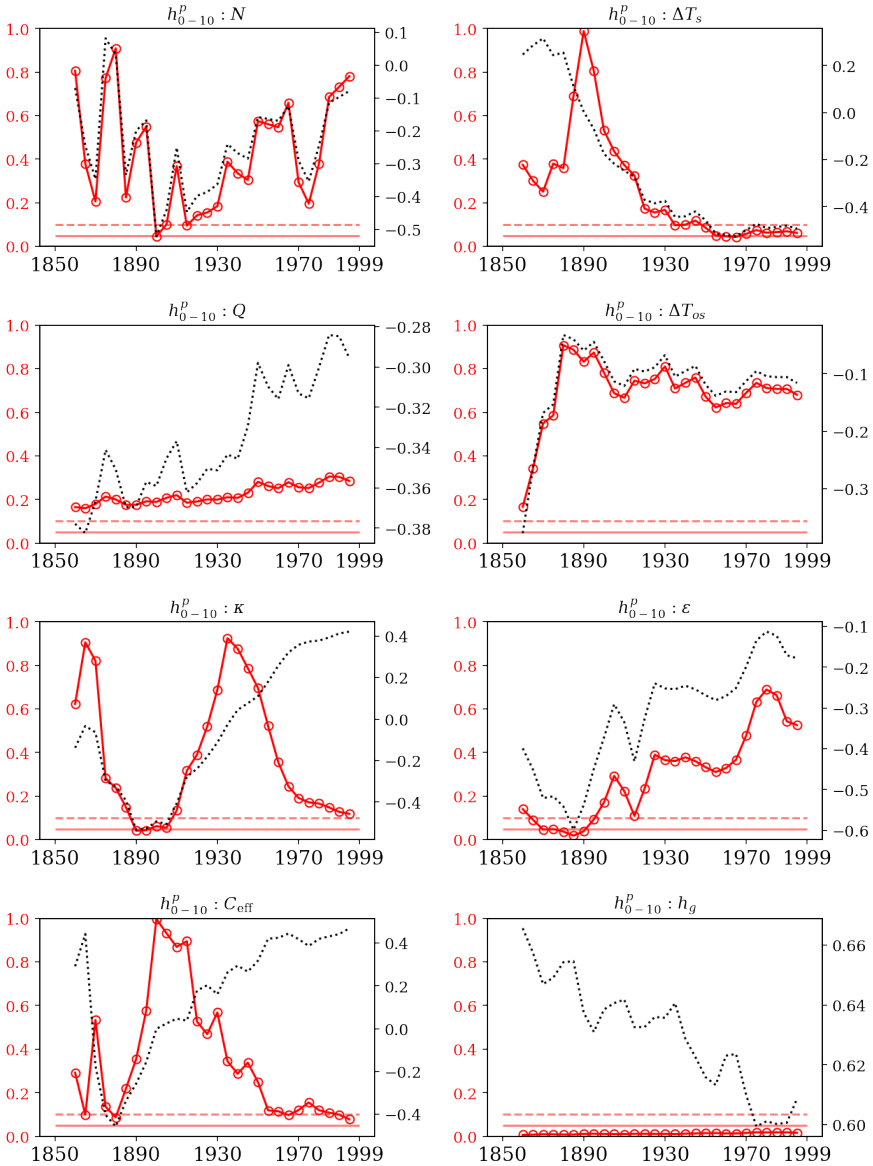

Figure A.1: Inter-ensemble correlations between the average subpolar MLD over years 1-10 and various climatic variables. The red line and circles denote the p value of the correlation, and the black dotten line denotes the r value. The red dashed line at bottom is the 10% significance threshold and the solid line is the 5% significance threshold.

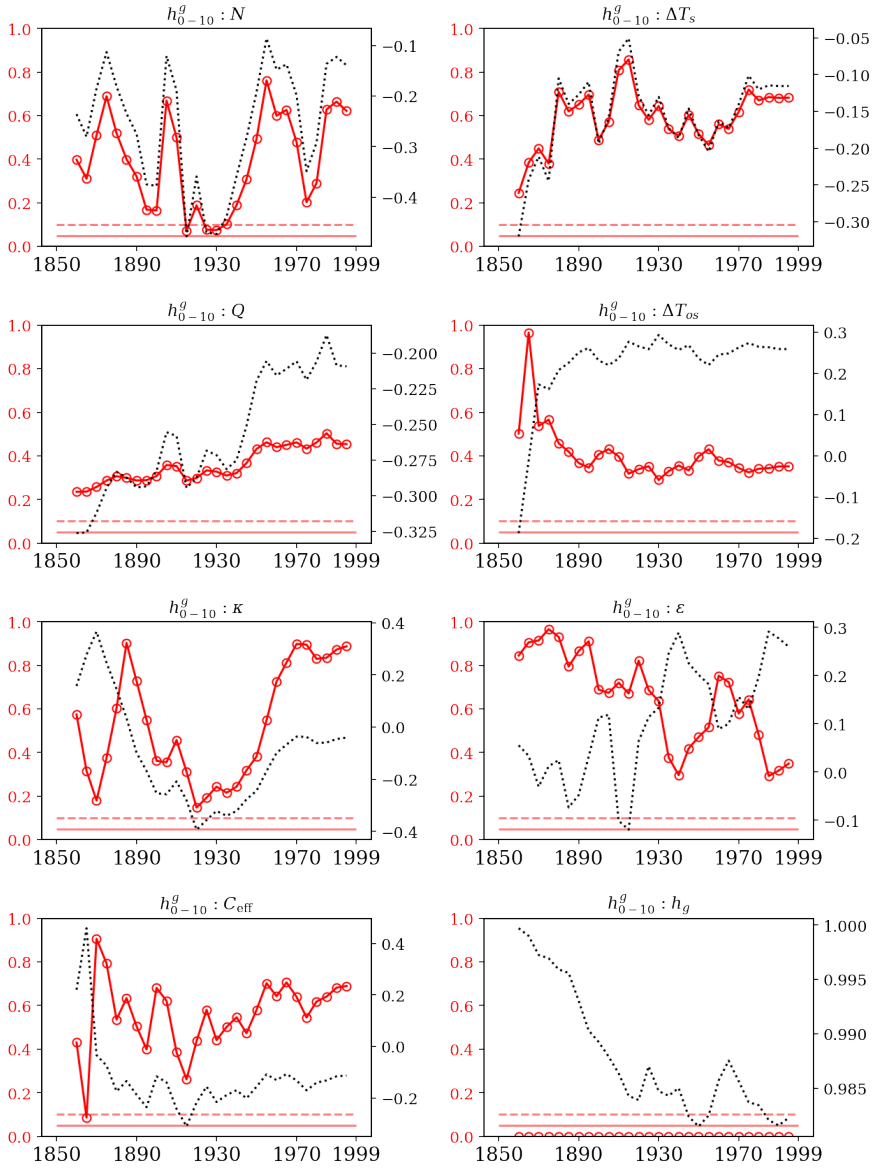

Figure A.2: Inter-ensemble correlations: average global MLD, years 1-10.

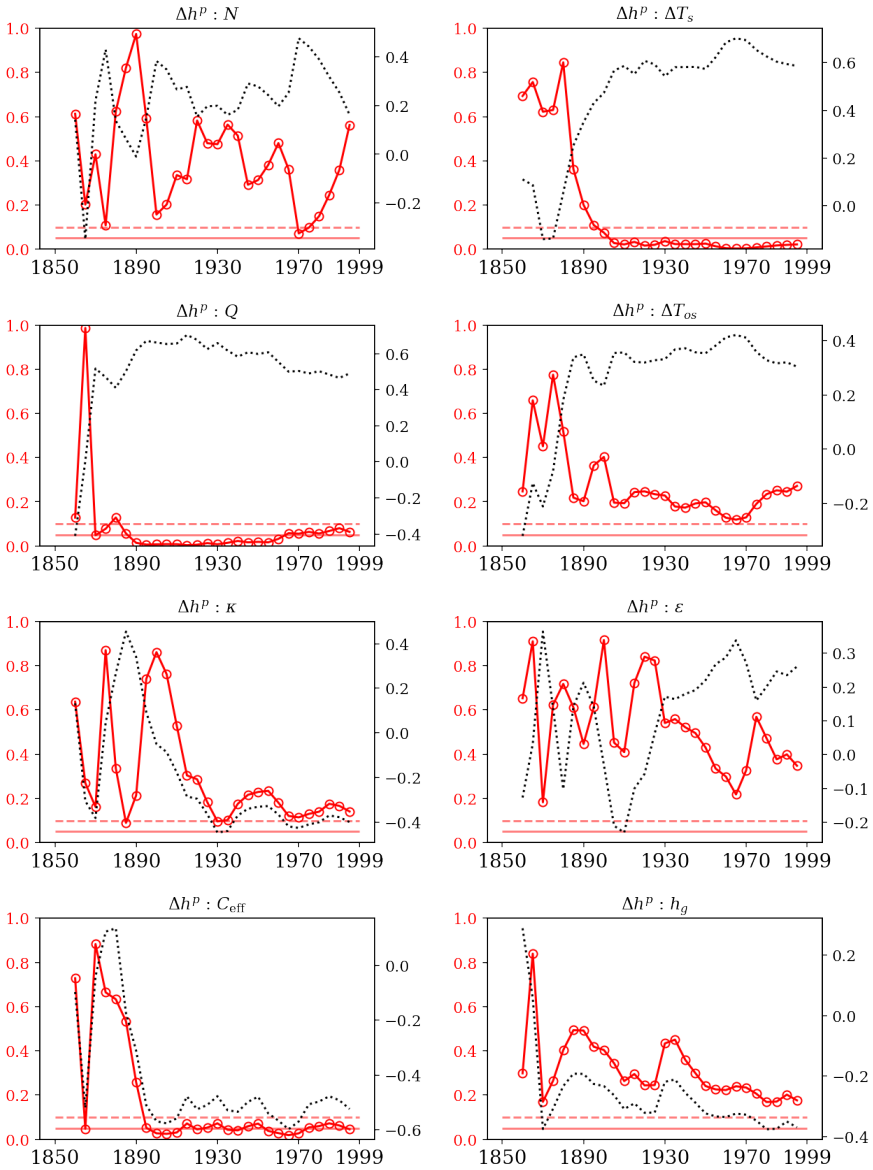

Figure A.3: Inter-ensemble correlations: change in average subpolar MLD from years 1-10.

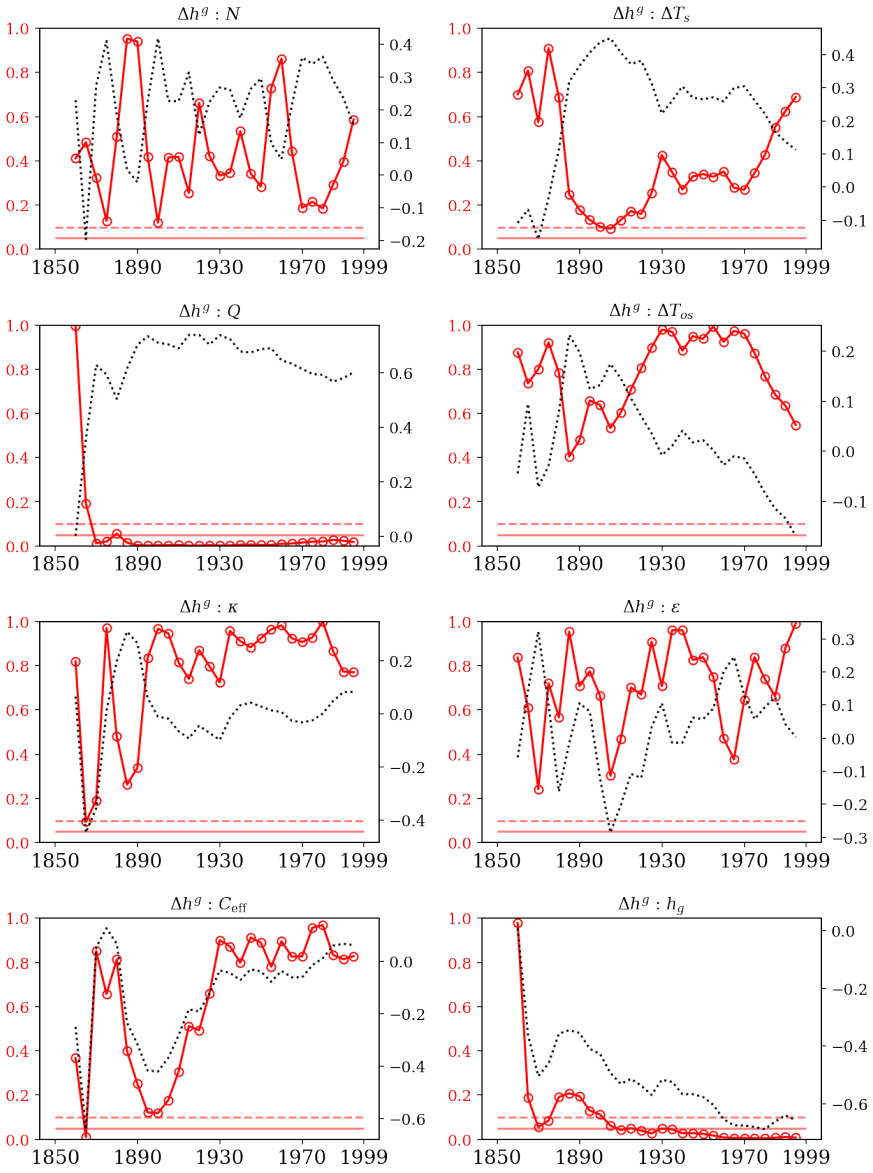

Figure A.4: Inter-ensemble correlations: change in average global MLD from years 1-10.

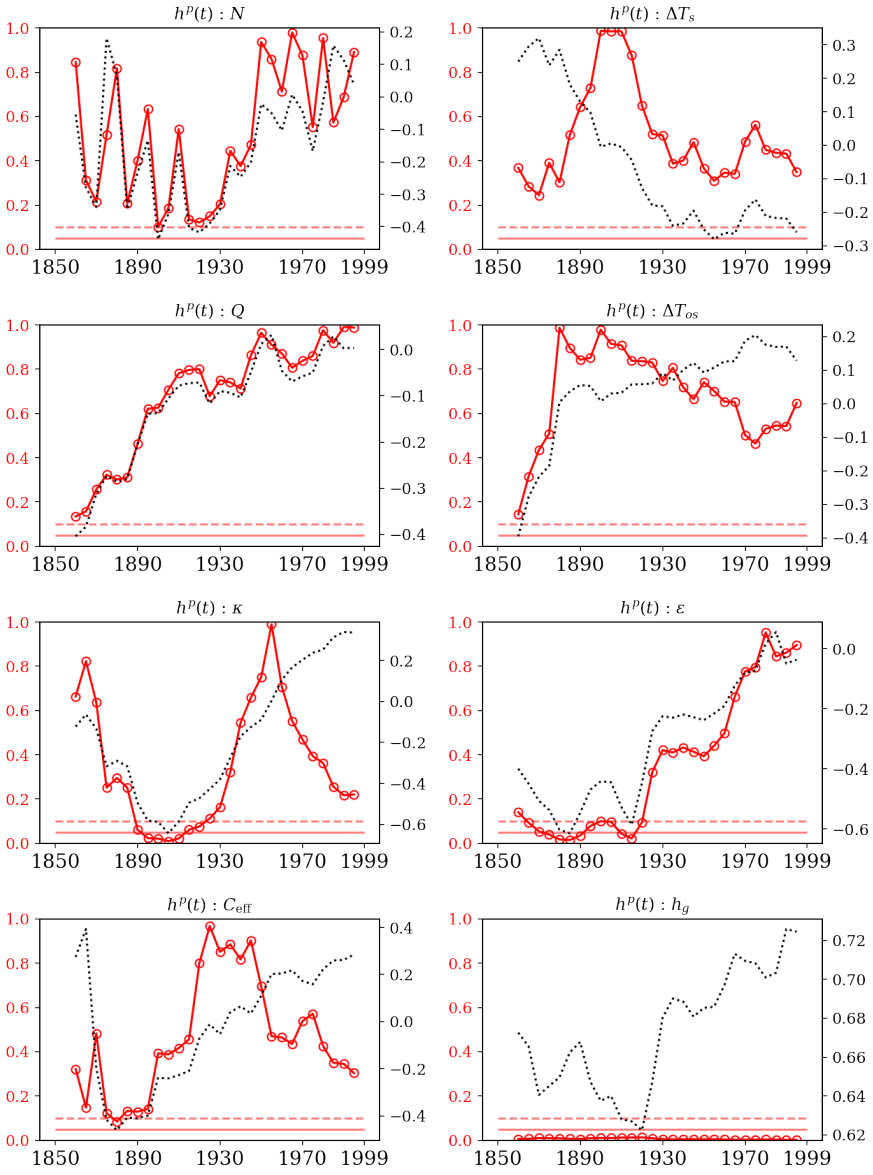

Figure A.5: Inter-ensemble correlations: subpolar MLD.

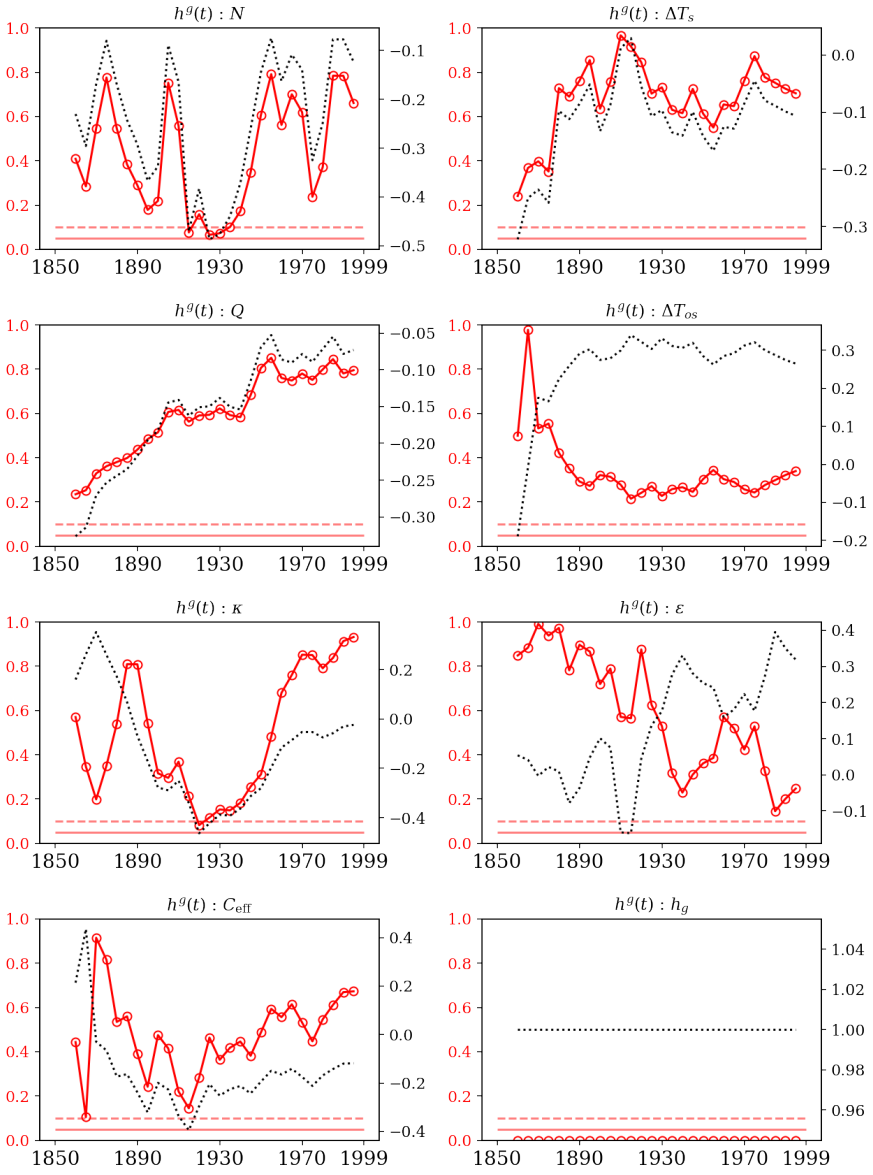

Figure A.6: Inter-ensemble correlations: global MLD.

Appendix B

Reproducing Geoffroy et al. (2013 *a*, *b*).

This section describes the procedure used to reproduce the results from Geoffroy et al. (2013*b*,*a*) for this ensemble of 16 CMIP6 AOGCMS. The resultant values are listed in each panel of figure B.2

For each model, beginning values for C_s, C_d, and γ were calculated using the `abrupt-4xCO2` runs and the analytical solutions to the simplified two-box model (equations (2.2.1) and (2.2.2)). The analytical solutions for each variable after a step forcing are derived in Geoffroy et al. (2013*b*) and allow for a direct fit based on the ΔT_s output. Then these values were refined and ϵ, λ, and $F_{4\times}$ were updated using the process described in Geoffroy et al. (2013*a*), which is briefly recreated below.

Fitting parameters with $\epsilon = 1$

First, fit ΔT to years 30-150 of `abrupt-4xCO2` using

$$\log\left(\Delta T_{eq} - \Delta T(t)\right) \approx \log \Delta T_{eq} + \log a_s - \frac{1}{\tau_s} t \tag{B.0.1}$$

to find the slow response timescale τ_s and the slow response scaling a_s. This solution, like those that follow, is derived analytically from the simple two-box model (no ϵ, or $\epsilon = 1$) under the assumption that the fast timescale $\tau_f \ll \tau_s$.

Use a similar fit to find the fast response:

$$\tau_f = t \log a_f - \log\left(1 - \frac{\Delta T}{\Delta T_{eq}} - a_s e^{t/\tau_s}\right). \tag{B.0.2}$$

Now calculate the the heat capacities and the heat coefficient γ:

$$C_s = \lambda/\left(\frac{a_f}{\tau_f} + \frac{a_s}{\tau_s}\right), \tag{B.0.3}$$

$$C_d = \lambda(\tau_s a_s + \tau_f a_f) - C_s, \tag{B.0.4}$$

$$\gamma = C_d/(\tau_s a_s + \tau_f a_f). \tag{B.0.5}$$

These parameters allow us to calculate the theoretical deep ocean temperature for step forcing with $\epsilon = 1$,

$$\Delta T_d(t) = \Delta T_{eq}(1 - \phi_f a_f e^{-t/\tau_f} - \phi_s a_s e^{-t/\tau_s}) \tag{B.0.6}$$

where

$$\phi_f = \frac{\lambda\tau_f - C_s}{C_d}, \quad \phi_s = \frac{\lambda\tau_s - C_s}{C_d}. \tag{B.0.7}$$

Iteration to find ϵ, λ and $F_{2\times}$

Each step takes the observed surface temperature change ΔT for the $4\times$ step forcing experiment, along with ϵ, λ and $F_{4\times}$ from the previous step. The starting values for λ an $F_{4\times}$ are those calculated via Gregory (2004) and $\epsilon^{(0)} = 1$.

First, evaluate $H^{(i)-1}$ using passed-in variables, by first finding γ and ΔT_d as above, giving

$$H^{(i)-1} = \gamma^{(i)-1}(\Delta T - \Delta T_d^{(i)-1}). \tag{B.0.8}$$

Second, perform a multilinear regression of N against T and H by combining equations (2.3.13) and (2.3.14) to obtain $\epsilon^{(i)}, \lambda^{(i)}$ and $F_{4\times}^{(i)}$:

$$N = F_{4\times}^{(i)} - \lambda^{(i)} T - [\epsilon^{(i)} - 1] H^{(i)-1}. \tag{B.0.9}$$

Finally, fit C_s, C_d, and γ as above. Although this fit is performed relative to the simpler model (i.e. $\epsilon = 1$), the answers converge quickly. After 10 or fewer iterations the values stabilized.

Note that this procedure relies on using a constant value for ϵ. As Yoshimori et al. (2016) point out, it is quite possible that the neither the real world nor AOGCMs behave like a constant-ϵ model. Finally, note that for all models with $\epsilon > 1$ the resulting estimates of $F_{2\times}$ and $\Delta T_{2\times}$ are both higher than the estimates using Gregory (2004). The only model in this ensemble with $\epsilon < 1$ is `CNRM-ESM2-1`.

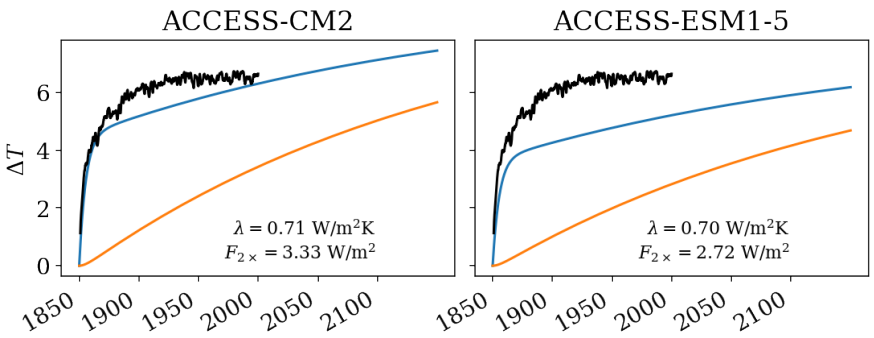

Figure B.1: An example showing the poor quality of the two-box model fit to `abrupt-4xCO2` without parameter optimization.

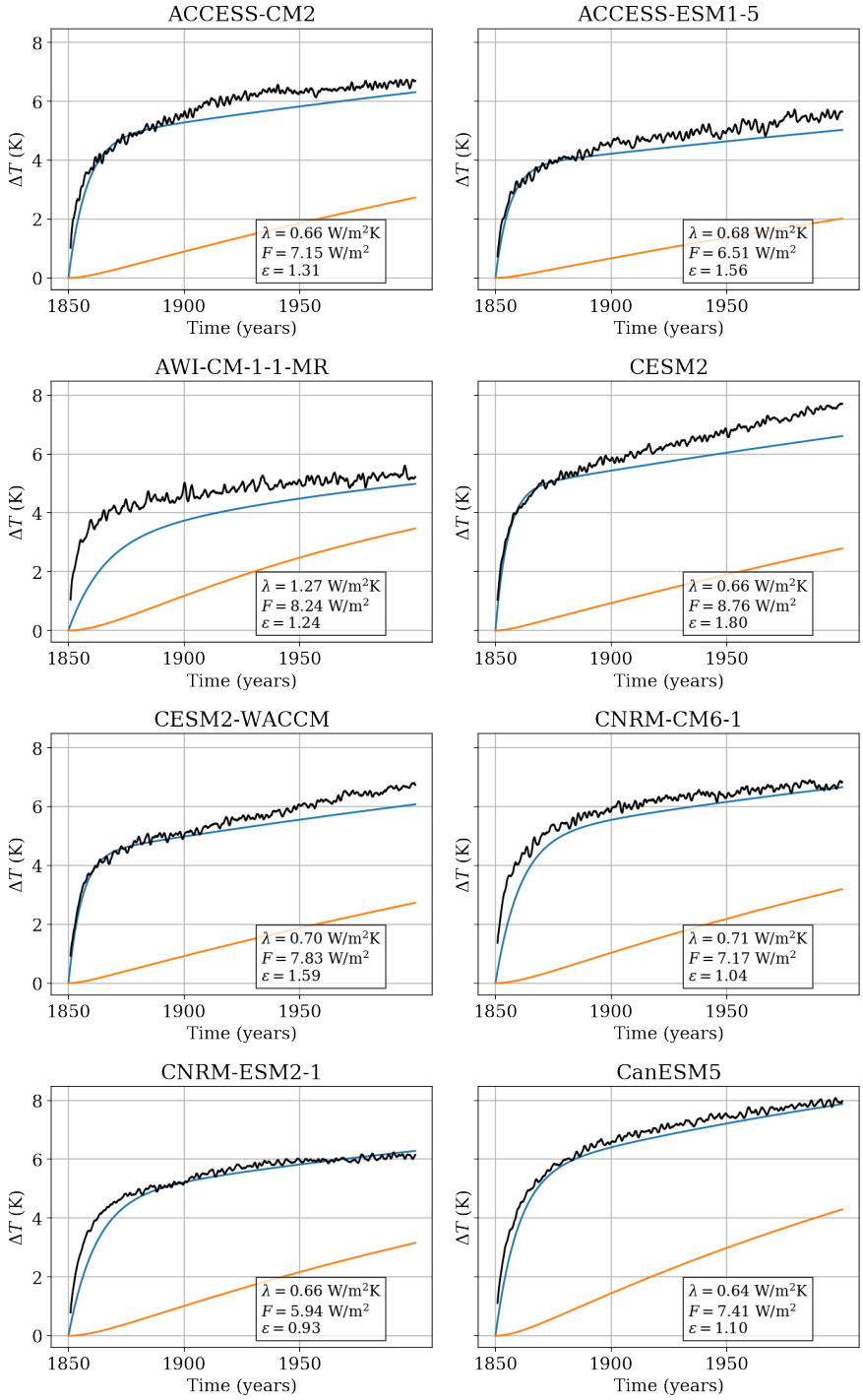

Figure B.2: The results from fitting the two-box linear system with ocean heat uptake efficacy ϵ to the model output from `abrupt-4xCO2` following the procedure in Geoffroy et al. (2013*b*,*a*). The modified fit parameters λ, $F = F_{4\times}$, and ϵ are labelled in a box inside each chart. Blue line: calculated surface temperature. Orange line: calculated deep ocean temperature.

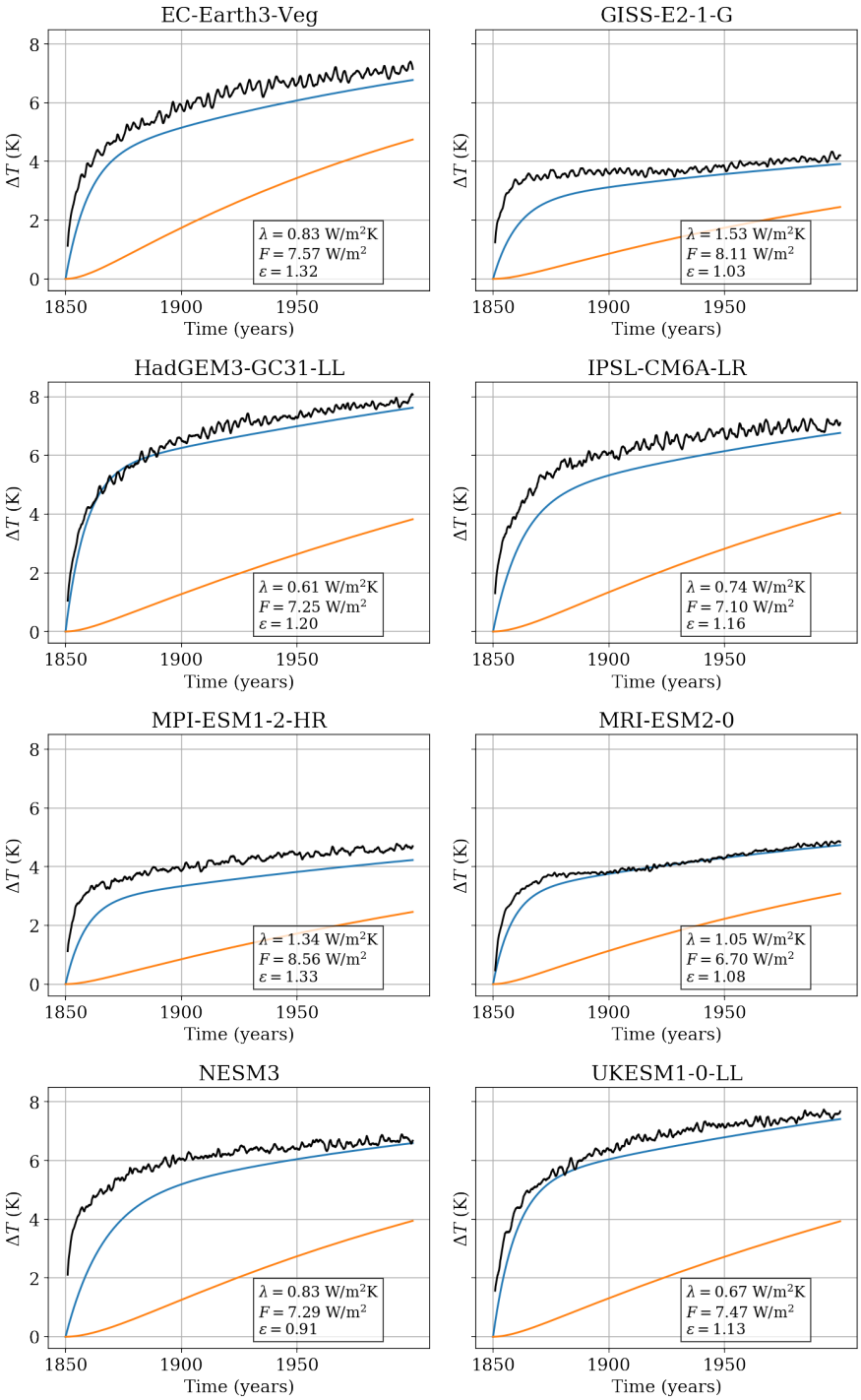

Continuation of figure B.2.

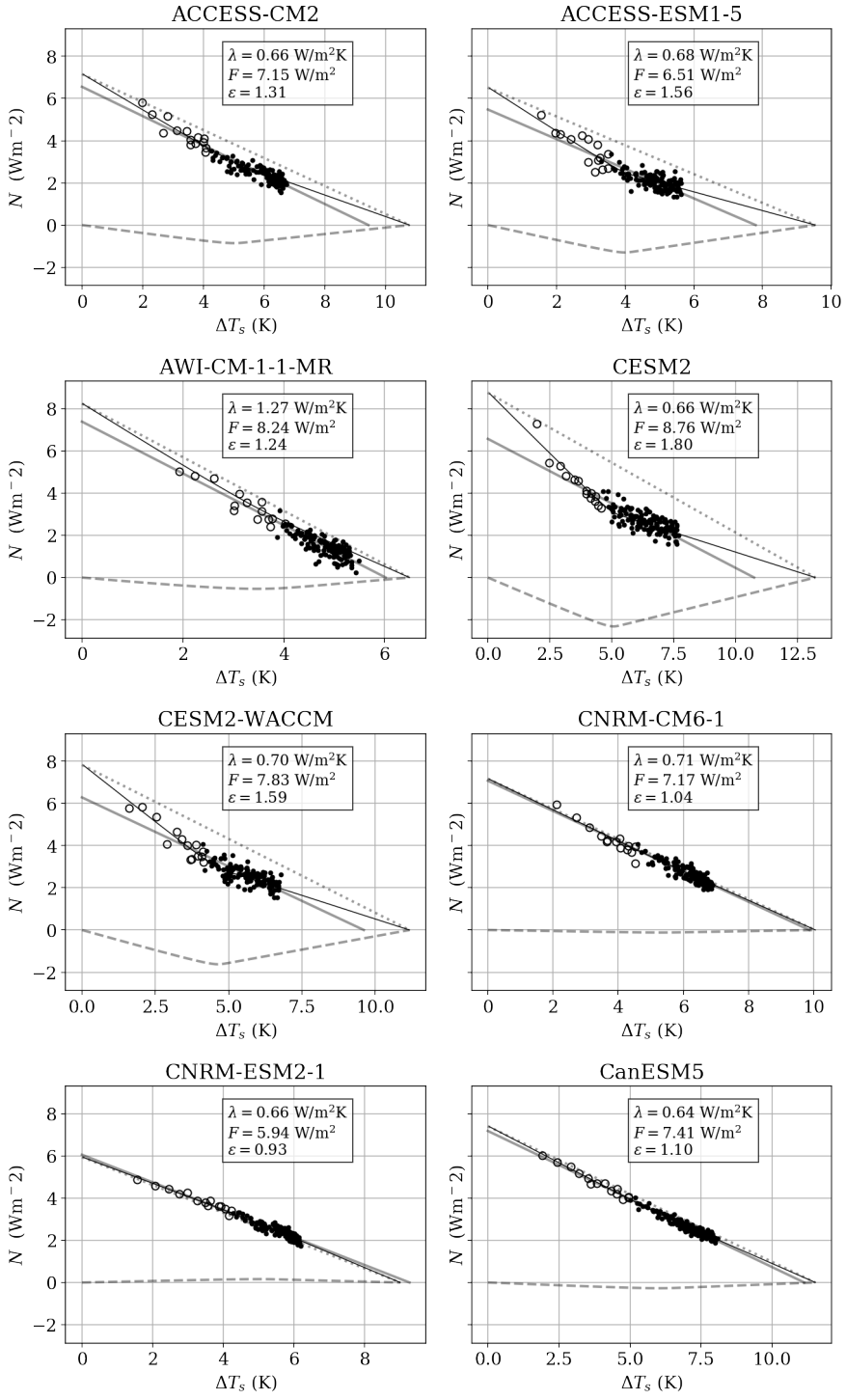

Figure B.3: The $N - \Delta T_s$ plots from the ensemble of 16 CMIP6 AOGCMs and ESMs. The circles are yearly averages over N and ΔT, and the hollow circles correspond to the first 15 years of the experiment. The thin black line indicates the two-box model fit. The dotted and dashed grey lines correspond to the $F - \lambda \Delta T_s$ and $(1 - \epsilon)H$ contributions to N. The thick grey line shows the trend calculated using Gregory (2004) methods. Note also that the format mimics the format found in Geoffroy et al. (2013*a*).

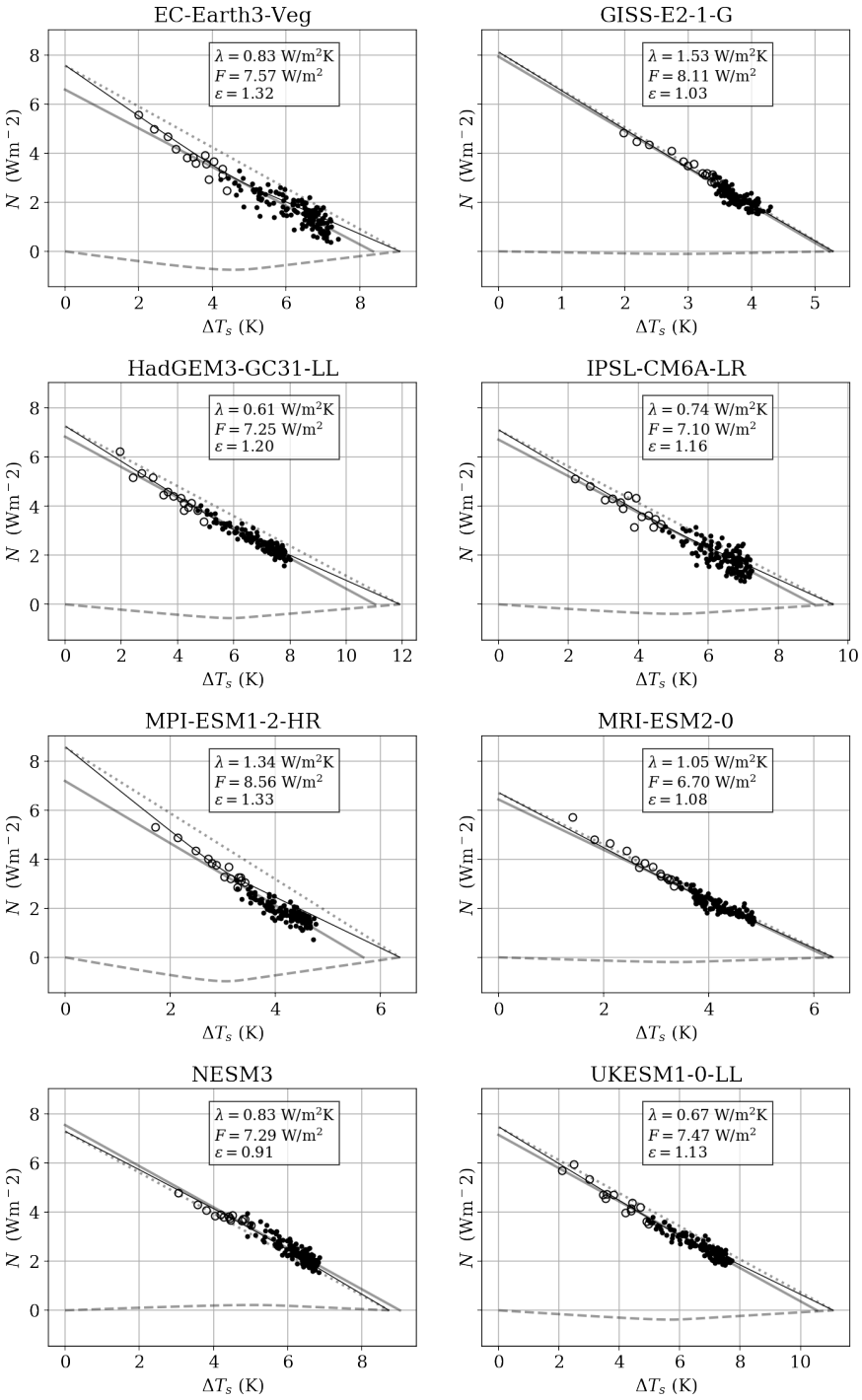

Continuation of figure B.3.

Bibliography

Allen, M. (2019), 'Lectures for Short Option 25: Physics of Climate Change'.

Andrews, D. G. (2010), *An introduction to atmospheric physics*, 2nd ed edn, Cambridge University Press, Cambridge ; New York.

Argo (2020), 'Argo float data and metadata from Global Data Assembly Centre (Argo GDAC)'. type: dataset.
URL: *https://www.seanoe.org/data/00311/42182/*

Armour, K. C., Bitz, C. M. and Roe, G. H. (2013), 'Time-Varying Climate Sensitivity from Regional Feedbacks', *Journal of Climate* **26**(13), 4518–4534.
URL: *http://journals.ametsoc.org/doi/10.1175/JCLI-D-12-00544.1*

Belcher, S. E., Grant, A. L. M., Hanley, K. E., Fox-Kemper, B., Van Roekel, L., Sullivan, P. P., Large, W. G., Brown, A., Hines, A., Calvert, D., Rutgersson, A., Pettersson, H., Bidlot, J.-R., Janssen, P. A. E. M. and Polton, J. A. (2012), 'A global perspective on Langmuir turbulence in the ocean surface boundary layer', *Geophysical Research Letters* **39**(18).
URL: *http://doi.wiley.com/10.1029/2012GL052932*

Boé, J., Hall, A. and Qu, X. (2009), 'Deep ocean heat uptake as a major source of spread in transient climate change

simulations', *Geophysical Research Letters* **36**(22). _eprint: https://onlinelibrary.wiley.com/doi/pdf/10.1029/2009GL040845.
URL: *http://agupubs.onlinelibrary.wiley.com/doi/abs/10.1029/2009GL040845*

Collins, M., Knutti, R., Arblaster, J., Dufresne, J.-L., Fichefet, T., Friedlingstein, P., Gao, X., Gutowski, W., Johns, T., Krinner, G., Shongwe, M., Tebaldi, C., Weaver, A. and Wehner, M. (2013), Long-term Climate Change: Projections, Commitments and Irreversibility, *in* T. Stocker, D. Qin, G.-K. Plattner, M. Tignor, S. Allen, J. Boschung, A. Nauels, Y. Xia, V. Bex and P. Midgley, eds, 'Climate Change 2013: The Physical Science Basis. Contribution of Working Group I to the Fifth Assessment Report of the Intergovernmental Panel on Climate Change', Cambridge University Press, Cambridge, United Kingdom and New York, NY, USA, pp. 1029–1136. Section: 12 Type: Book Section.
URL: *www.climatechange2013.org*

Craik, A. D. D. and Leibovich, S. (1976), 'A rational model for Langmuir circulations', *Journal of Fluid Mechanics* **73**(3), 401–426.

Donohoe, A., Frierson, D. M. W. and Battisti, D. S. (2014), 'The effect of ocean mixed layer depth on climate in slab ocean aquaplanet experiments', *Climate Dynamics* **43**(3-4), 1041–1055.
URL: *http://link.springer.com/10.1007/s00382-013-1843-4*

Eyring, V., Bony, S., Meehl, G. A., Senior, C. A., Stevens, B., Stouffer, R. J. and Taylor, K. E. (2016), 'Overview of the Coupled Model Intercomparison Project Phase 6 (CMIP6) experimental design and organization', *Geoscientific Model Development* **9**(5), 1937–1958. Publisher: Copernicus GmbH.
URL: *https://www.geosci-model-dev.net/9/1937/2016/*

Flato, G., Marotzke, J., Abiodun, B., Braconnot, P., Chou, S., Collins, W., Cox, P., Driouech, F., Emori, S., Eyring, V., Forest, C., Gleckler, P., Guilyardi, E., Jakob, C., Kattsov, V., Reason, C. and Rummukainen, M. (2013), Evaluation of Climate Models, *in* T. Stocker, D. Qin, G.-K. Plattner, M. Tignor, S. Allen, J. Boschung, A. Nauels, Y. Xia, V. Bex and P. Midgley, eds, 'Climate Change 2013: The Physical Science Basis. Contribution of Working Group I to the Fifth Assessment Report of the Intergovernmental Panel on Climate Change', Cambridge University Press, Cambridge, United Kingdom and New York, NY, USA, pp. 741–866. Section: 9 Type: Book Section.

URL: *www.climatechange2013.org*

Frankignoul, C. and Hasselmann, K. (1977), 'Stochastic climate models, Part II Application to sea-surface temperature anomalies and thermocline variability', *Tellus* **29**(4), 289–305.

URL: *https://www.tandfonline.com/doi/full/10.3402/tellusa.v29i4.11362*

Geoffroy, O., Saint-Martin, D., Bellon, G., Voldoire, A., Olivié, D. J. L. and Tytéca, S. (2013*a*), 'Transient Climate Response in a Two-Layer Energy-Balance Model. Part I: Analytical Solution and Parameter Calibration Using CMIP5 AOGCM Experiments', *Journal of Climate* **26**(6), 1841–1857.

URL: *http://journals.ametsoc.org/doi/10.1175/JCLI-D-12-00195.1*

Geoffroy, O., Saint-Martin, D., Bellon, G., Voldoire, A., Olivié, D. J. L. and Tytéca, S. (2013*b*), 'Transient Climate Response in a Two-Layer Energy-Balance Model. Part II: Representation of the Efficacy of Deep-Ocean Heat Uptake and Validation for CMIP5 AOGCMs', *Journal of Climate* **26**(6), 1859–1876.

URL: *http://journals.ametsoc.org/doi/10.1175/JCLI-D-12-00196.1*

Gettelman, A., Hannay, C., Bacmeister, J. T., Neale, R. B., Pendergrass, A. G., Danabasoglu, G., Lamarque, J., Fasullo, J. T., Bailey, D. A., Lawrence, D. M. and Mills, M. J. (2019), 'High Climate Sensitivity in the Community Earth System Model Version 2 (CESM2)', *Geophysical Research Letters* **46**(14), 8329–8337.
URL: *https://onlinelibrary.wiley.com/doi/abs/10.1029/2019GL083978*

Gregory, J. M. (2000), 'Vertical heat transports in the ocean and their effect on time-dependent climate change', *Climate Dynamics* **16**(7), 501–515. Place: Berlin/Heidelberg Publisher: Springer-Verlag.

Gregory, J. M. (2004), 'A new method for diagnosing radiative forcing and climate sensitivity', *Geophysical Research Letters* **31**(3), L03205.
URL: *http://doi.wiley.com/10.1029/2003GL018747*

Gregory, J. M. and Forster, P. M. (2008), 'Transient climate response estimated from radiative forcing and observed temperature change', *Journal of Geophysical Research* **113**(D23), D23105.
URL: *http://doi.wiley.com/10.1029/2008JD010405*

Hansen, J., Sato, M., Kharecha, P. and von Schuckmann, K. (2011), 'Earth's energy imbalance and implications', *Atmospheric Chemistry and Physics* **11**(24), 13421–13449.
URL: *https://www.atmos-chem-phys.net/11/13421/2011/*

Hasselmann, K. (1976), 'Stochastic climate models Part I. Theory', *Tellus* **28**(6), 473–485.
URL: *https://www.tandfonline.com/doi/full/10.3402/tellusa.v28i6.11316*

Held, I. M., Winton, M., Takahashi, K., Delworth, T., Zeng, F. and Vallis, G. K. (2010), 'Probing the Fast and Slow Components of Global Warm-

ing by Returning Abruptly to Preindustrial Forcing', *Journal of Climate* **23**(9), 2418–2427.
URL: *http://journals.ametsoc.org/doi/10.1175/2009JCLI3466.1*

Huang, C. J., Qiao, F. and Dai, D. (2014), 'Evaluating CMIP5 simulations of mixed layer depth during summer', *Journal of Geophysical Research: Oceans* **119**(4), 2568–2582.
URL: *https://agupubs.onlinelibrary.wiley.com/doi/abs/10.1002/2013JC009535*

Kantha, L. H. and Anne Clayson, C. (2004), 'On the effect of surface gravity waves on mixing in the oceanic mixed layer', *Ocean Modelling* **6**(2), 101–124.
URL: *https://linkinghub.elsevier.com/retrieve/pii/S1463500302000628*

Li, Q., Reichl, B. G., Fox-Kemper, B., Adcroft, A. J., Belcher, S. E., Danabasoglu, G., Grant, A. L. M., Griffies, S. M., Hallberg, R., Hara, T., Harcourt, R. R., Kukulka, T., Large, W. G., McWilliams, J. C., Pearson, B., Sullivan, P. P., Roekel, L. V., Wang, P. and Zheng, Z. (2019), 'Comparing Ocean Surface Boundary Vertical Mixing Schemes Including Langmuir Turbulence', *Journal of Advances in Modeling Earth Systems* **11**(11), 3545–3592.
URL: *https://agupubs.onlinelibrary.wiley.com/doi/abs/10.1029/2019MS001810*

Li, Q., Webb, A., Fox-Kemper, B., Craig, A., Danabasoglu, G., Large, W. G. and Vertenstein, M. (2016), 'Langmuir mixing effects on global climate: WAVEWATCH III in CESM', *Ocean Modelling* **103**, 145–160.
URL: *https://linkinghub.elsevier.com/retrieve/pii/S1463500315001407*

Marshall, J. and Plumb, R. A. (2008), *Atmosphere, ocean, and climate dynamics: an introductory text*, number v. 93 *in* 'International geophysics

series', Elsevier Academic Press, Amsterdam ; [Burlington, MA]. OCLC: ocn166317541.

Murphy, J. (1995), 'Transient response of the Hadley Center coupled ocean-atmosphere model to increasing carbon dioxide. Part III: Analysis of global-mean response using simple models', *Journal of Climate, Boston, MA* **8**(3), 496–514.

Nijsse, F. J. M. M., Cox, P. M. and Williamson, M. S. (2020), An emergent constraint on Transient Climate Response from simulated historical warming in CMIP6 models, preprint, Earth system change: climate prediction.
URL: *https://www.earth-syst-dynam-discuss.net/esd-2019-86/*

Taylor, K. E., Stouffer, R. J. and Meehl, G. A. (2012), 'An Overview of CMIP5 and the Experiment Design', *Bulletin of the American Meteorological Society* **93**(4), 485–498.
URL: *http://journals.ametsoc.org/doi/abs/10.1175/BAMS-D-11-00094.1*

Thorpe, S. (2004), 'Langmuir Circulation', *Annual Review of Fluid Mechanics* **36**(1), 55–79.

Thorpe, S. A. (2007), *An introduction to ocean turbulence*, Cambridge University Press, Cambridge; New York. OCLC: 772458320.
URL: *https://doi.org/10.1017/CBO9780511801198*

Vallis, G. K. (2017), *Atmospheric and Oceanic Fluid Dynamics: Fundamentals and Large-Scale Circulation*, 2 edn, Cambridge University Press, Cambridge.
URL: *http://ebooks.cambridge.org/ref/id/CBO9781107588417*

Vallis, G. K. (2019), *Essentials of atmospheric and oceanic dynamics*, Cambridge University Press, Cambridge [etc. OCLC: 1089723642.

van den Bremer, T. S. and Breivik, O. (2018), 'Stokes drift', *Philosophical Transactions of the Royal Society A: Mathematical, Physical and Engineering Sciences* **376**(2111), 20170104.
URL: *https://royalsocietypublishing.org/doi/10.1098/rsta.2017.0104*

Watanabe, M., Kamae, Y., Yoshimori, M., Oka, A., Sato, M., Ishii, M., Mochizuki, T. and Kimoto, M. (2013), 'Strengthening of ocean heat uptake efficiency associated with the recent climate hiatus: HEAT UPTAKE EFFICIENCY AND RECENT HIATUS', *Geophysical Research Letters* **40**(12), 3175–3179.
URL: *http://doi.wiley.com/10.1002/grl.50541*

Winton, M., Adcroft, A., Dunne, J. P., Held, I. M., Shevliakova, E., Zhao, M., Guo, H., Hurlin, W., Krasting, J., Knutson, T., Paynter, D., Silvers, L. G. and Zhang, R. (2020), 'Climate Sensitivity of GFDL's CM4.0', *Journal of Advances in Modeling Earth Systems* **12**(1).
URL: *https://onlinelibrary.wiley.com/doi/abs/10.1029/2019MS001838*

Winton, M., Takahashi, K. and Held, I. M. (2010), 'Importance of Ocean Heat Uptake Efficacy to Transient Climate Change', *Journal of Climate* **23**(9), 2333–2344.
URL: *http://journals.ametsoc.org/doi/10.1175/2009JCLI3139.1*

Wyngaard, J. C. (2010), *Turbulence in the atmosphere*, Cambridge University Press, Cambridge, UK ; New York. OCLC: ocn422765274.

Yoshimori, M., Watanabe, M., Shiogama, H., Oka, A., Abe-Ouchi, A., Ohgaito, R. and Kamae, Y. (2016), 'A review of progress towards understanding the transient global mean surface temperature response to radiative perturbation', *Progress in Earth and Planetary Science* **3**(1), 21.

URL: *http://progearthplanetsci.springeropen.com/articles/10.1186/s40645-016-0096-3*